Results in Engineering 29 (2026) 109934

Contents lists available at ScienceDirect

Results in Engineering

journal homepage: www.sciencedirect.com/journal/results-in-engineering

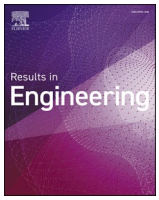

Research paper

Synergistic mechanisms of biochar and fly ash on water retention and crack suppression in molybdenum tailings soil under wet–dry cycles

Binbin Yang [1,3], Mingming Hu [b,*]

[a] School of Civil Engineering, Xuchang University, Xuchang, Henan 461000, China
[b] School of Geological Engineering and Geomatics, Chang'an University, Xi'an, Shanxi 710000, China
[c] School of Civil Engineering, Wuhan University, No.299 Bayi Road, Wuhan, Hubei 430072, China

ARTICLE INFO

Keywords:
Wet–dry cycle
Molybdenum tailings
Biochar
Fly ash
Soil crack control

ABSTRACT

Molybdenum tailings soil lacks organic matter and biological activity, making it highly prone to compaction and unsuitable for plant survival. Drought and heavy rainfall events further exacerbate its degradation. To improve soil quality, fly ash and biochar were incorporated and subjected to three years of natural field curing without artificial intervention. To investigate the synergistic effects of fly ash and biochar on soil remediation, indoor simulations of five consecutive wet–dry cycles were conducted. Image processing techniques and fractal dimension analysis were employed to quantitatively assess changes in soil water retention and crack development. Results indicate that the combined application of fly ash and biochar significantly suppressed soil crack formation and expansion, reducing crack density and fractal dimension while enhancing soil water-holding capacity. The treatment with 10% fly ash and 4% biochar showed the greatest improvement, increasing residual moisture content by 105.64% and reducing fractal dimension and crack rate by 28.43% and 41.75%, respectively, after the first cycle compared to the control. This mechanism primarily arises from the combined effects of biochar pore adsorption and fly ash hydration cementation, which jointly enhance aggregate stability, block rapid water evaporation pathways, and mitigate structural degradation during wet–dry cycles. This study provides the first integrated assessment of biochar–fly ash synergy in molybdenum tailings soil using fractal crack analysis. Larger-scale statistical validation and field trials are needed to confirm practical feasibility.

1. Introduction

Molybdenum tailings exhibit severe soil degradation, characterized by pH values >9, soil compaction, and elevated concentration of heavy metals such as lead, cadmium, and arsenic. These pollutants inhibit plant growth, damage surrounding topography (Fig. 1), and degrade soil ecological functions. In recent years, soil degradation has intensified due to the combined effects of increasingly extreme weather events and human activities [1,2]. Soil erosion is mainly caused by natural factors, such as mudslides and landslides triggered by heavy rainfall, as well as by human activities, including excessive land use and industrial mining [3,4].

Human activities destroy vegetation, leading to soil exposure, dehydration, shrinkage, and crack formation under high temperatures, which increase permeability and susceptibility to erosion [5,6]. This process renders topsoil more susceptible to rainfall erosion, thereby accelerating fertility loss and degradation. Industrial and mining operations cause heavy metal accumulation beyond the environmental carrying capacity, thereby inhibiting plant growth, altering microbial community structures, and destabilizing ecosystems [7–9]. Molybdenum tailings ponds exemplify these degradation processes. Excess molybdenum is toxic to plants, hindering growth and potentially causing mortality, while simultaneously impairing soil microbial diversity and function and disrupting ecological balance [10]. Under extreme rainfall conditions, pollutants such as molybdenum can migrate through soil cracks to surrounding areas, resulting in broader contamination and ecological degradation [11,12]. To address this challenge, numerous studies have explored remediation pathways for molybdenum-contaminated tailings soils.

Soil remediation technologies can be broadly categorized into three main types: chemical remediation, biological remediation, and physical remediation. Chemical remediation is primarily achieved through the

* Corresponding author at: School of Geological Engineering and Geomatics, State Key Laboratory for Geomechanics and Deep Underground Engineering, Chang an University, 1 University Rd, Xi'an 710000, China
E-mail addresses: 20191002@xcu.edu.cn (B. Yang), hmm@chd.edu.cn (M. Hu).

https://doi.org/10.1016/j.rineng.2026.109934
Received 28 November 2025; Received in revised form 16 February 2026; Accepted 4 March 2026
Available online 5 March 2026

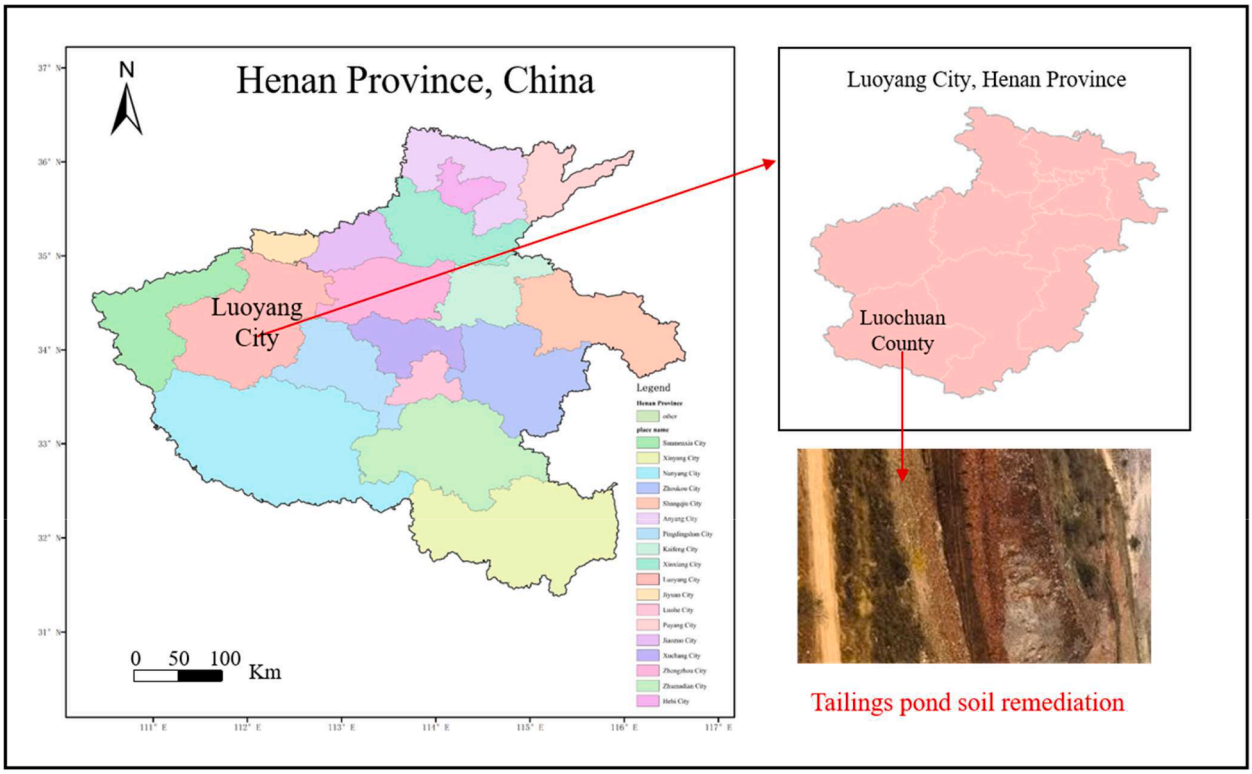

Fig. 1. Location and mining area of molybdenum tailings.

addition of soil amendments, including biochar, fly ash, lime, and fibers, to exploit their adsorption, precipitation, cementation, oxidation, and flocculation-promoting mechanisms [13–17]. This process effectively immobilizes heavy metals within the soil matrix, restricts their migration potential, and transforms them into less toxic and more insoluble forms, thereby reducing associated pollution risks. Bioremediation primarily relies on synergistic interactions between vegetation and soil microorganisms to enhance soil physicochemical properties and functional stability. Phytoremediation facilitates contaminant removal through plant-driven photosynthetic processes that uptake and accumulate heavy metals from the surrounding environment [18–20]. Physical remediation treats contaminated soil through separation, replacement, or burial, producing immediate effects but requiring substantial engineering input and incurring high implementation costs [21,22]. Overall, physical and biological remediation approaches involve longer treatment cycles and higher implementation costs, whereas chemical remediation is more widely applied in practice due to its comparatively simpler operation and rapid effectiveness. However, traditional single remediation methods often prove insufficient for complex systems such as molybdenum tailings, which are characterized by high alkalinity and the coexistence of multiple contaminant types [23]. This unique combination of high alkalinity and mixed contamination necessitates remediation strategies that extend beyond those conventionally applied to acidic or single-pollutant mine soils. For instance, purely physical methods are often prohibitively expensive; phytoremediation is difficult to establish in heavily polluted environments; and single chemical amendment materials fail to produce sustained improvements in soil structure. Therefore, there is urgent need to develop integrated remediation strategies achieve heavy metal passivation, soil structure improvement, and ecological function restoration.

Soil undergoes volumetric shrinkage and forms interconnected crack networks during dehydration, representing a common physical degradation phenomenon in arid and semi-arid regions [24]. These cracks accelerate soil moisture evaporation, increase soil permeability, compromise structural integrity, and significantly influence soil stability and pollutant migration pathways [25,26]. Traditional assessment methods cannot accurately quantify these complex, irregular crack morphologies. Fractal theory can quantitatively characterized the complexity, connectivity, and evolutionary patterns of crack networks using parameters such as fractal dimension [27]. Unlike conventional indicators such as crack width or crack density, fractal parameters can effectively characterize structural complexity and disorder, thereby providing quantitative insights into soil structure stability. Applying fractal geometry to soil crack research enables quantitative analysis of the relationships between crack development and parameters such as time scale, thereby providing a scientific basis for evaluating soil stability and formulating targeted crack prevention measures.

Previous studies indicate that biochar can enhance soil porosity and enzymatic activity, promote plant growth, improve plant tolerance to extreme weather conditions, and effectively mitigate soil pollution [28,29]. As a relatively inert material, biochar also promotes the growth and activity of soil microbial communities [30]. Its abundant recalcitrant carbon components exhibit strong carbon sequestration capacity, thereby helping to increase soil moisture content under arid conditions [31,32]. In soil remediation applications, biochar effectively immobilizes both organic and inorganic pollutants by adsorbing heavy metals such as copper, mercury, cobalt, and chromium, thereby reducing their mobility and bioavailability and mitigating associated environmental toxicity. This immobilization effect is further enhanced by biochar's abundant polar functional groups and aromatic structures [33,34]. Biochar can undergo specific adsorption or coordination reactions with molybdate ions via surface oxygen-containing functional groups, thereby enhancing molybdate immobilization through surface complexation and electrostatic attraction [35] Additionally, biochar incorporation can regulate soil pH and redox potential, creating a microenvironment conducive to the transformation of molybdenum from soluble to residual forms, thereby improving the overall management efficiency of molybdenum pollution [36]. Furthermore, fine biochar particles can fill soil pores, thereby inhibiting crack development and reducing soil water loss under drought conditions [37,38].

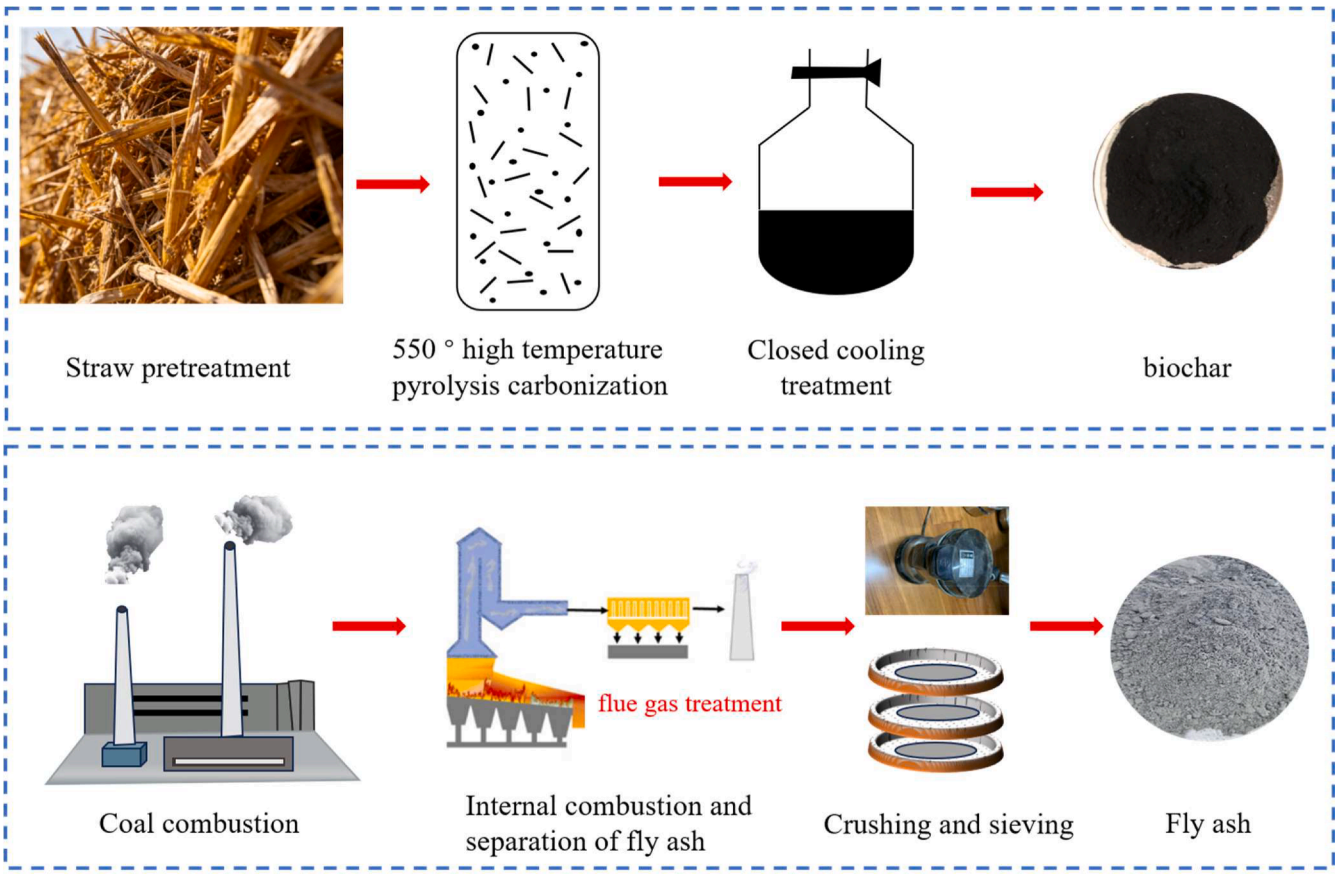

Fig. 2. Process flow of biochar preparation and the harmless recovery of fly ash.

Fly ash, a common industrial byproduct containing various metallic elements and mineral components, is widely used as an adsorbent material in environmental applications. Its fine particles can occupy soil voids, thereby enhancing internal friction, improving particle interlocking, and increasing overall structural stability [39]. Fly ash also improves soil water retention, increases soil organic carbon content, and supplies macronutrients and micronutrients that are essential for plant growth [40]. For the remediation of molybdenum pollution, oxides and minerals such as calcium, iron, and aluminum present in fly ash can form insoluble molybdates with molybdate ions via co-precipitation, thereby achieving long-term immobilization [41]. In acidic soils, fly ash can regulate soil pH, reduce the leaching of harmful metals, and synergistically remediate lead contamination when combined with biochar [42–45]. Upon interaction with water, fly ash forms cementitious substances that further fill soil pores, suppress crack development, and enhance soil water-holding capacity [46,47]. The production process of biochar and the recycling pathway of fly ash are illustrated in Fig. 2.

Therefore, to elucidate the coupling mechanism between fly ash and biochar under wet–dry cycle conditions, this study quantitatively analyzed soil cracking behavior using indoor simulation experiments combined with digital image processing techniques. Previous studies have examined biochar or fly ash individually for soil improvement and heavy metal immobilization, and a few have combined both in acidic agricultural soils, but none have systematically quantified their synergistic effects on crack evolution and water retention in highly alkaline molybdenum tailings under repeated wet–dry cycles. Therefore, this work provides the first integrated assessment of biochar–fly ash synergy on both hydraulic behavior (evaporation stages, residual moisture) and crack network complexity (fractal dimension, crack rate, node density) in molybdenum-contaminated tailings. The objective of this study is to: (1) To quantify the synergistic effects of biochar and fly ash on water retention in molybdenum contaminated tailings; (2) To determine optimal biochar-fly ash ratios for crack suppression under wet dry cycling. The research hypothesis is that: (1) the combination of fly ash and biochar can improve water retention more effectively than using a single component alone; (2) The optimal ratio to minimize cracks is 10 % fly ash and 4 % biochar; (3) Fly ash and biochar reduce the rate of sample water evaporation, and the potential mechanisms involve the synergistic regulation of Cementing substances fly ash and water transport through the porous structure of biochar.

2. Materials and methods

2.1. Materials

The soil samples for this experiment were collected from the experimental fields and natural soil in the molybdenum mining area of Luanchuan County, Luoyang City, Henan Province. This area is located in the Wuyun Mountain range and has a warm-temperate continental monsoon climate with significant diurnal temperature variations. All the samples were naturally maintained on-site for three years before sampling, without any artificial intervention during this period, to ensure the natural stability of the soil structure during the wet–dry cycle.

Soil samples were uniformly collected from the experimental field within a 4 $m \times 4$ m area at a depth of 15 cm. The collected samples were subsequently divided into 24 plots, comprising 12 material treatment combinations and 12 corresponding control groups. The experimental treatments were classified into three main categories based on the content of fly ash: 0 %, 5 %, and 10 %. Within each category, biochar was incorporated at different concentrations (0 %, 1 %, 2 %, and 4 %), resulting in a total of 12 distinct treatments. The control groups were designed to be identical to the experimental treatments in all aspects

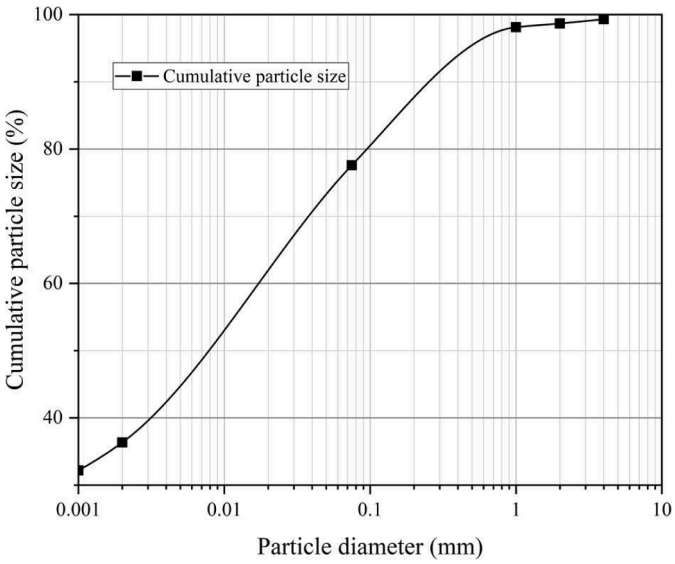

Fig. 3. Particle size distribution curve of the soil samples.

Table 1
Physical Properties of Low Plasticity Clay.

specific gravity (Gs)	Natural water content (%)	Plastic Limit (%)	Liquid Limit (%)	Shrinkage Limit (%)	Molybdenum (mg/kg)
2.72	12.56	19.12	37.34	9.42	0.16

Table 2
Physical properties of the treated fly ash.

Dry density	Particle size (μm)	color	Sio_2(%)	Al_2o_3(%)	Fe_2o_3(%)
2.23	<80	grey	41.2	18.42	4.68

Table 3
Content of Harmful Metals in Fly Ash.

As	Pb	Cd	Cr	Hg	*Ni*
2mg/kg	0.1 mg/kg	0.12 mg/kg	20 mg/kg	0.05 mg/kg	8 mg/kg

except for material addition. All experimental and control areas underwent the same three-year natural maintenance process, after which subsequent laboratory analyses were conducted. For each of the 24 field plots, two representative subsamples were collected after three years of natural conditioning. This paper focuses on the lab cyclic tests using field-aged soil, and detailed field monitoring results will be reported elsewhere. All subsequent laboratory wet–dry cycling tests were performed on these field-aged soils ($n = 2$ specimens per treatment). No additional amendments were added during laboratory preparation.

The collected soil samples were sealed with plastic films and transported to the laboratory for further processing. After air-drying at room temperature, visible plant residues and gravel particles larger than 2 mm were removed from the samples. The samples were then passed through a 2 mm standard sieve to obtain homogeneous base soil. Subsequently, key physical parameters were measured, after which the samples were dried and sieved for further analysis to obtain the particle size distribution curve (Fig. 3). The basic physical properties of the soil samples are summarized in Table 1.

The fly ash used in this experiment was sourced from the power plant operated by Luan Chuan County He Hai New Energy Luan Chuan Co., Ltd. China. Fly ash consists predominantly of fine, glassy particles and commonly contains potentially harmful metals such as mercury (Hg), lead (Pb), arsenic (As), and nickel (Ni). Although the fly ash used in this experiment had been treated by the company, it was still necessary to test the collected fly ash to ensure it would not contaminate the soil. The physical properties of the fly ash are presented in Table 2, while Table 3 summarizes the concentrations of harmful metals in the fly ash, all of which meet the regulatory standards for soil application.

Biochar is a carbon-rich material derived from the pyrolysis of various waste feedstocks—such as agricultural residues, wood, and plant stems—under anoxic or low-oxygen conditions at temperatures typically below 700 °C. It is characterized by a high specific surface area, considerable adsorption capacity, and remarkable stability. The biochar used in this experiment was manufactured by Luoyang Zhao Tuo Carbon Technology Co., Ltd., China. The biochar was manufactured by pyrolyzing agricultural crop residues, primarily wheat straw, at 460 °C for 5 h. Subsequently, the biochar was air-dried at 50 °C, mechanically pulverized, and sieved through a 0.2 mm mesh prior to the measurement of its basic physicochemical properties (Table 4).

2.2. Methods

The 24 soil samples were naturally air-dried, gently pulverized, and passed through a 2-mm sieve. From each sieved sample, 100 g of dry soil was mixed with 102 g of water to form a circular disc measuring 25 cm in diameter and 3 cm in height, resulting in a saturated slurry with a moisture content of 102 %. The prepared slurry was vibrated for 30 min using a vibrator to remove air bubbles, then sealed and cured for 2 days.

To simulate the natural environment characterized by alternating rainfall and drying, this experiment was conducted in a multifunctional climate chamber (ZHS), with the temperature set to 26 °C and the relative humidity maintained at 50 %. The cured specimens were placed on an electronic balance inside the ZHS, with a high-resolution digital camera fixed vertically above the specimens. At 2 h intervals, the computer-controlled camera and electronic balance recorded crack im-

Table 5
Wet dry cycle protocol specification.

Parameter	Specification	Justification
Drying phase temperature	26 °$C \pm 2$ °C	Actual shallow soil temperature in arid areas
Drying phase RH	45±5 %	Relative humidity of natural environment in arid regions
Drying duration	140h	Low and constant evaporation rate
Wetting phase intensity	24h(13.4 mm)	Simulates moderate rainfall event
Wetting phase duration	24h	Intermittent wetting, with water completely penetrating into the soil.
Cycle duration (one complete cycle)	7days	Total drying + wetting time
Total cycles tested	5 cycles	Balances acceleration with practical duration
Chamber light conditions	24-hour illumination	Control variables; Constant temperature

Table 4
Basic Properties of Biochar.

Pyrolysis temperature (°C)	Ash content (%)	Specific surface area (m2/g)	Bulk density (g/cm3)	C (%)	N (%)	o (%)	H (%)
460	11.52	106.7	0.46	76	1.1	5.67	3.2

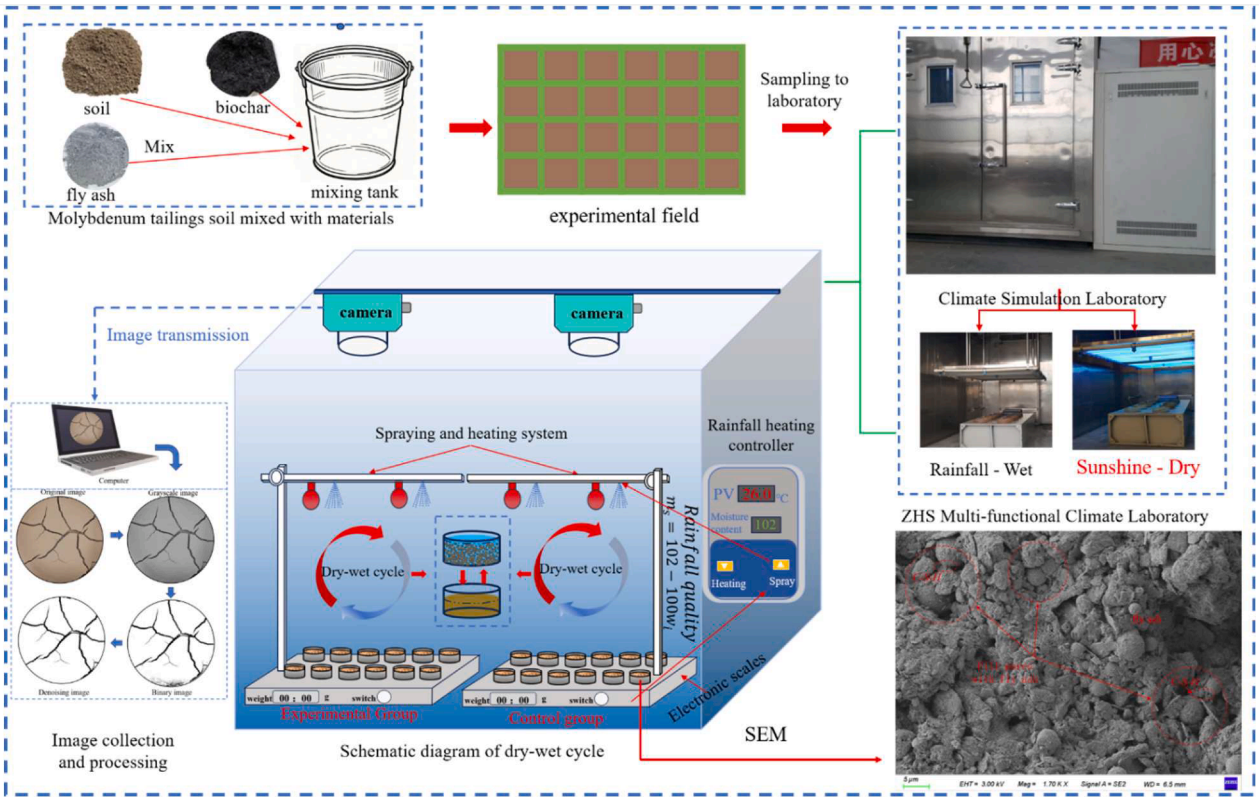

Fig. 4. Experimental flowchart.

Table 6
Framework for analyzing fractal dimension of soil cracks.

Fractal dimension range	Definition and Physical Meaning	Application in Soil Fracture Research
The closer the fractal dimension (FD) value is to 1.0, the more simple, straight and smooth the fracture outline or boundary shape becomes. On the contrary, the closer the D value is to 2.0, the more irregular the fracture outline is, the more branches it has, and the poorer its structural stability.	Fractal dimension is an extension of the concept of integer dimensions in Euclidean geometry (such as 1-dimensional lines and 2-dimensional planes), used to quantify the self-similarity or space-filling degree of complex and irregular shapes under scale changes. Its core lies in describing the complexity of the geometric figure: the higher the D value, the more irregular the shape is, the more complex its structure is, and the stronger its space-filling ability is.	When there are no cracks on the soil surface, the theoretical value of the fractal dimension of the crack network is 1, indicating good integrity and high stability of the soil structure. As the cracks develop, the fractal dimension value increases, reflecting the aggravation of soil damage and the decline of stability. When the fractal dimension approaches 2, the cracks are highly interwoven and the network fills the plane, indicating that the soil structure has been severely fragmented and degraded.

ages and specimen mass, respectively, until crack development stabilized. Subsequently, rainfall treatments were applied using the ZHS to simulate multiple rainfall events. The specific parameters of the dry–wet cycle are summarized in Table 5. Water was replenished according to the residual moisture content of each specimen to restore the initial moisture content to 102 % of its reference value. The amount of replenished water required for each specimen was calculated using Formula (1).

$$m_s = 102 - 100w_i \quad (1)$$

Among these variables, m_s represents the amount of water required to achieve the target moisture content (102 %), and w_i denotes the current moisture content of the i sample.

This wet–dry cycle was repeated five consecutive times. The overall experimental procedure is illustrated schematically in Fig. 4.

2.3. Image processing techniques

During image acquisition, raw images often contain noise arising from factors such as uneven illumination, background interference, and variations in exposure levels. To obtain more accurate and reliable crack analysis results, image preprocessing is therefore required. The image-processing workflow primarily consists of three sequential steps: gray-scale conversion, image binarization, and noise reduction.

On the processed, high-clarity images, crack development can be systematically observed and analyzed. Cracks initially initiate form on the specimen surface, appearing as several primary traces. Subsequently, these traces gradually deepen, widen, and elongate, eventually propagating across the entire specimen surface. Cracks exhibiting these characteristics are defined as primary cracks. Relatively finer cracks that branch from primary cracks are termed secondary cracks. Furthermore, all finer cracks generated from secondary cracks, as well as those formed subsequently, are uniformly defined as tertiary cracks. Based on the topological characteristics of crack intersections, crack nodes can be further classified as follows: Primary crack nodes refer to intersection points where four or more cracks converge, forming a multi-directional cross-like structure. Secondary crack nodes are defined as convergence points of three cracks, forming a Y-shaped structure. Tertiary crack nodes are characterized by a T-shaped connection, in which a relatively shallow terminal crack connects to only one other crack and does not intersect with additional cracks.

Color images present challenges in crack detection due to high computational demands, increased interference with crack identification, and elevated noise levels. Therefore, color images must undergo

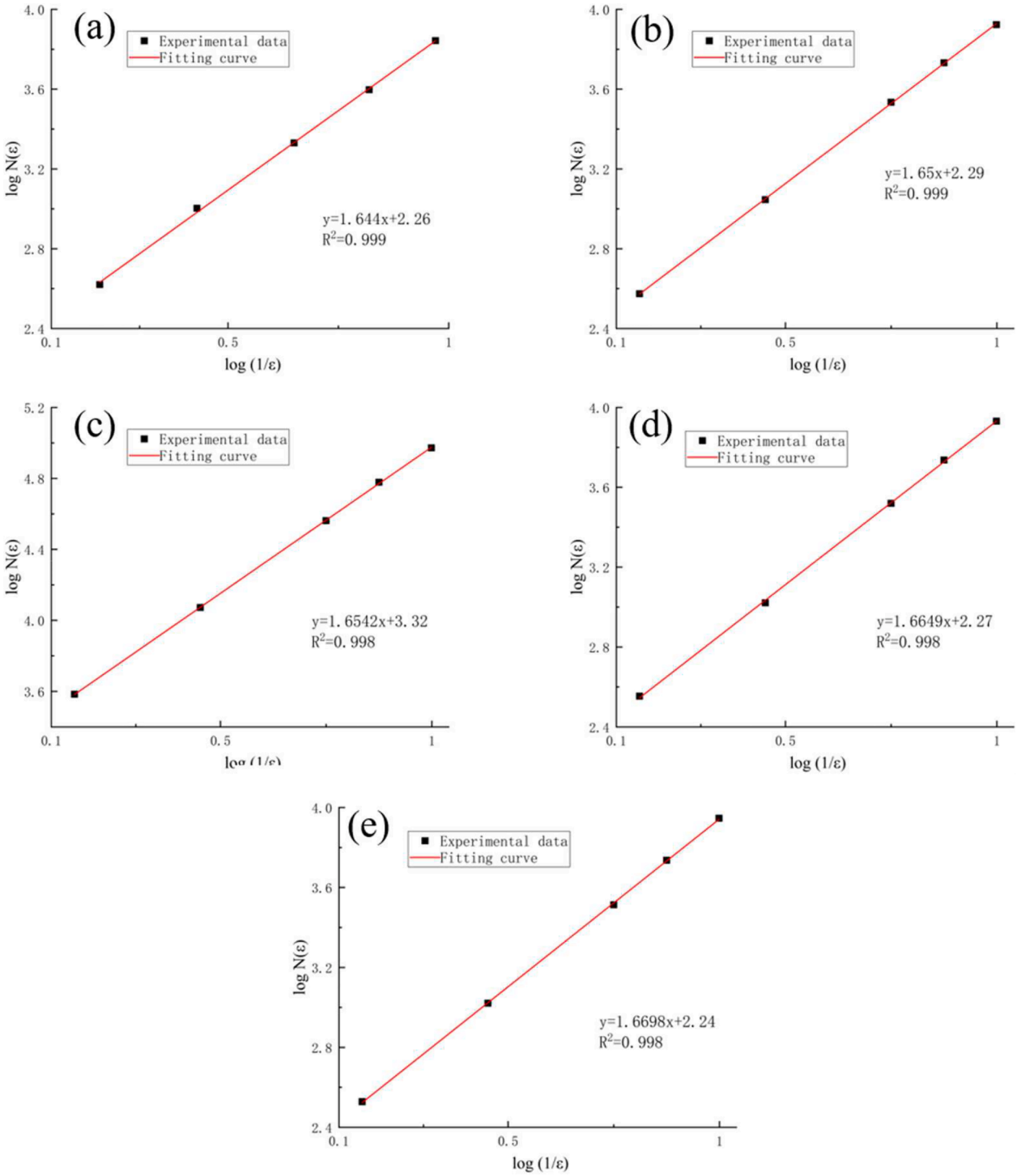

Fig. 5. Fractal dimension calculation process.

grayscale conversion prior to further analysis. This process converts the RGB channels into a single grayscale channel using a weighted averaging algorithm.

$$Gray = 0.3 * R + 0.6 * G + 0.1 * B \tag{2}$$

Grayscale images fail to clearly highlight crack features, and the grayscale background can interfere with crack identification during parameter analysis. Therefore, grayscale images require binarization processing. Binarization involves selecting an appropriate threshold T (Utilize the Otsu method to automatically calculate the optimal global threshold T for each grayscale image) to segment the image, converting continuous grayscale information into a black and white image. Black and white regions are separated according to the following formula. Areas below threshold T are classified as black, while those above threshold T are classified as white, thereby completing the binarization process. During the binarization process, noise may arise from isolated black and white pixels and from edges that are not accurately thresholded. A neighborhood-based thresholding approach is therefore employed to remove such noise, thereby yielding a clearer and more continuous crack image.

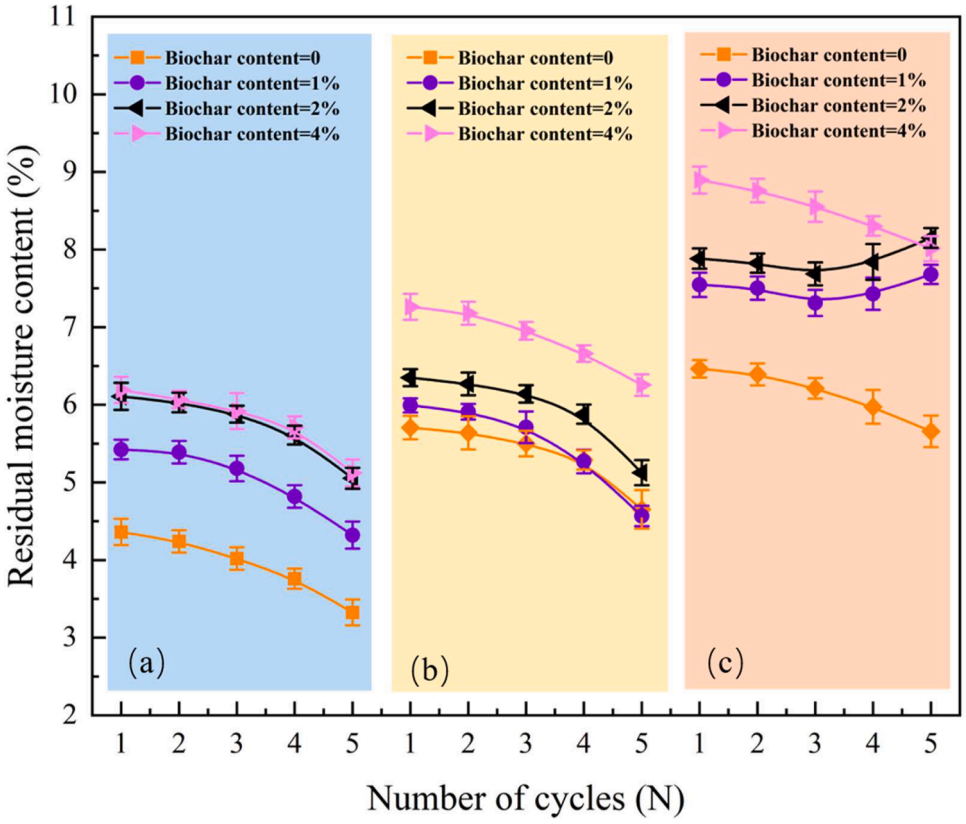

Fig. 6. Residual moisture content of different treatments across wet–dry cycles. Error bars represent SEM ($n = 2$) (a) Fly ash content maintained at 0 %; (b) fly ash content maintained at 5 %; (c) fly ash content maintained at 10 %.

$$W(\mathrm{x},\mathrm{y}) = \begin{cases} 0, G(\mathrm{x},\mathrm{y}) < T \\ 255, G(\mathrm{x},\mathrm{y}) \geq T \end{cases} \tag{3}$$

2.4. Calculation of crack characteristic parameters

Fractal dimension (FD) is utilized as a mathematical descriptor of complex geometric irregularity, enabling accurate characterization of the disorder, complexity, and self-similarity exhibited by soil surface cracks (see Table 6 for details). Current methods for calculating fractal dimension include: the compass dimension method, multiple fractal analysis, the Sandbox method, the box-counting method, and the variance method. For image analysis, the box-counting method is simpler and more applicable. This method involves setting different sizes ε to cover the image, obtaining the number of boxes N(ε) covering the image, and using a double logarithmic curve to derive the fractal dimension D. We conducted two independent box counting analysis processes on all images. When the goodness of fit (R2) obtained from both the fitting and classification calculations exceeds 0.98, the corresponding fractal dimension is considered valid, and the fitted curve is shown in Fig. 5. The formulas used to calculate the fractal dimension (D) and the coefficient of determination (R^2) are given as follows:

Log (N_p) represents the logarithm of the model-predicted value, which is calculated using Formula 5.

$$D = \lim_{\varepsilon \to 0} \frac{\log \mathrm{N}(\varepsilon)}{\log\left(\frac{1}{\varepsilon}\right)} \tag{4}$$

$$R2 = 1 - \frac{\sum (\log \mathrm{N}(\varepsilon) - \log \mathrm{Np})}{\sum (\log \mathrm{N}(\varepsilon) - \overline{\log \mathrm{N}(\varepsilon)})} \tag{5}$$

$$\log \mathrm{Np} = -D \log \mathrm{N}(\varepsilon) + C \tag{6}$$

The Crack rate represents the total length of Cracks per unit area. A higher Crack rate indicates greater soil permeability but poorer stability, making the soil more susceptible to failure. The formula used to calculate the crack rate (C) is given as follows:

$$C = \frac{\sum \mathrm{l_i}}{\mathrm{A}} \tag{7}$$

The total area of the image under analysis is defined as the cumulative length of cracks within the area A.

The mass of water required to achieve 100 % moisture content in the specimen was calculated using the following formula:

$$m\omega = \frac{0.01 \times (\omega - \omega_0)}{1 + 0.01\omega_0} \times m_0 \tag{8}$$

Target moisture content. This refers to the moisture content of the sample after drying, representing the quality of the dried sample.

The relative evaporation rate (E) of the sample was calculated based on the measurement interval and the corresponding change in mass.

$$E = \frac{\Delta \mathrm{m}}{\Delta \mathrm{t}} \tag{9}$$

Δm is the mass difference at the initial evaporation interval of the sample, g; Δt is the time interval, h, which is 2 h in this paper.

3. Result

3.1. The regulating effect of biochar powder and coal ash on the water retention of molybdenum tailings soil under dry-wet cycling conditions

In this study, samples containing 0 % biochar and 0 % fly ash were designated as the control group. Fig. 7 presents the evaporation rate curves of moisture content for the different samples over time. The moisture content of each sample initially decreased in a linear manner

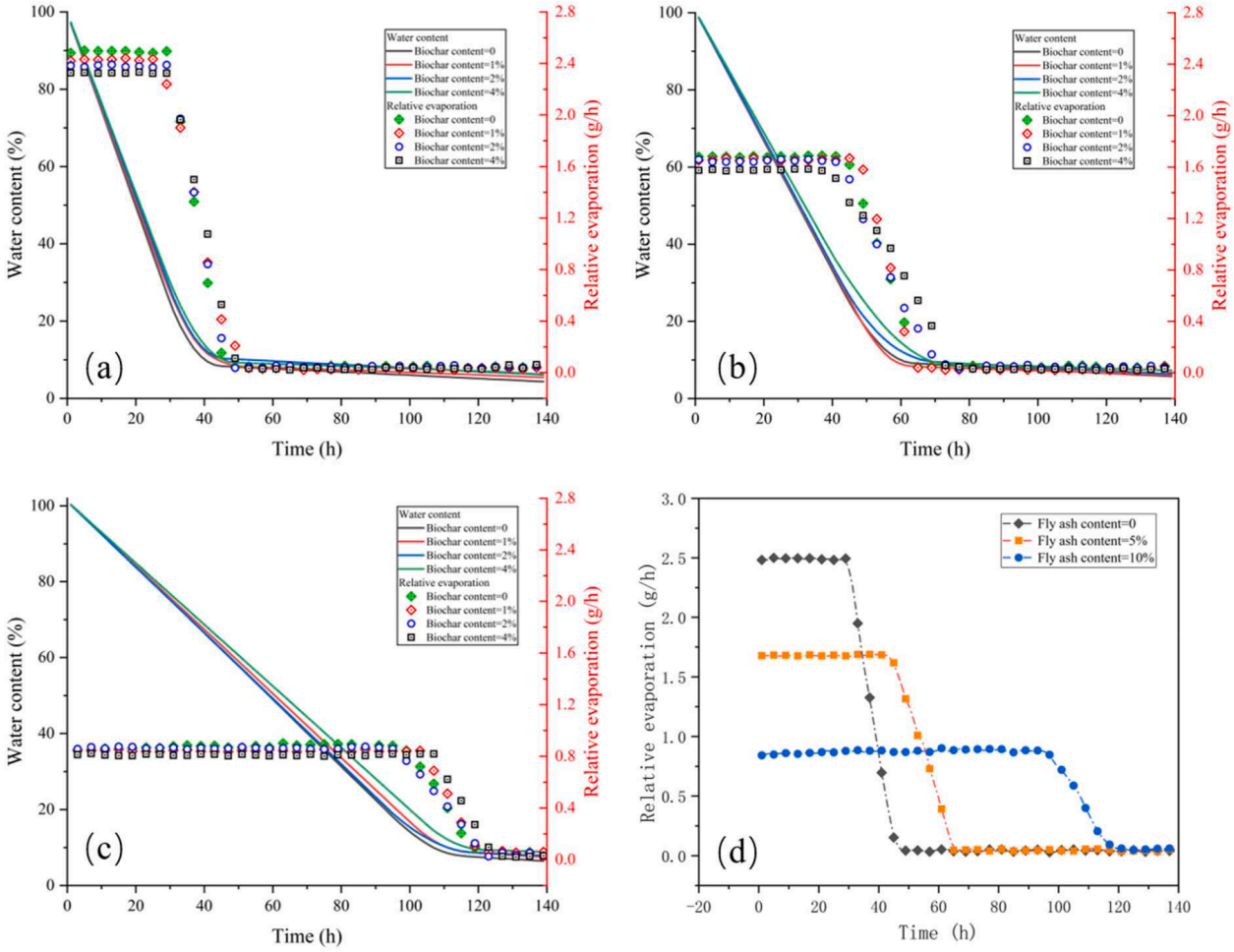

Fig. 7. Changes in soil evaporation rate and moisture content over time. (a) Fly ash content maintained at 0 %; (b) fly ash content maintained at 5 %; (c) fly ash content maintained at 10 %; (d) biochar content maintained at 0 %.

and subsequently reached a stable state. As shown in Fig. 7, the evaporation rate of each sample was initially maintained at a relatively high level and then rapidly declined to a low-rate stable evaporation stage. The moisture evaporation process of the samples can be divided into three distinct stages: a stable rapid evaporation stage, an evaporation deceleration stage, and a residual evaporation stage.

As shown in Fig. 6a, when the fly ash content remained at 0 %, and under the same number of dry–wet cycles, the final residual moisture content of the samples increased with increasing biochar content. After the first dry-wet cycle, the residual moisture content of the control group was 4.326 ± 0.168 %; for the samples with biochar contents of 1 %, 2 %, and 4 %, the residual moisture contents were 5.424 ± 0.125 %, 6.108 ± 0.174 %, and 6.192 ± 0.167 % respectively. Compared to the control group, the residual moisture contents of the samples with 1 %, 2 %, and 4 % biochar after the first cycle increased by 25.38 %, 41.19 %, and 43.11 % respectively. With the increase in the number of dry-wet cycles, the residual moisture content of all samples showed a downward trend. Taking the control group as an example, after the fifth dry-wet cycle, the residual moisture content of the sample dropped to 3.325 %, a decrease of 23.15 % compared to 4.326 % after the first cycle. While for the samples with 1 %, 2 %, and 4 % biochar, the residual moisture contents after the fifth cycle were 4.321 ± 0.175 %, 5.054 ± 0.135 %, and 5.123 ± 0.173 % respectively, and compared with the data after the first cycle, their residual moisture contents decreased by 20.34 %, 17.26 %, and 17.26 % respectively, all smaller than the 23.15 % decrease of the control group. The addition of biochar significantly enhance the water retention capacity of the samples, effectively slowed water loss, and improved their ability to retain moisture under alternating wet–dry conditions. As shown in Fig. 7a, when the fly ash content remained at 0 %, the first-stage evaporation rate of the samples decreased with increasing biochar content. Compared with the control group, samples containing 1 % biochar did not exhibit significant differences in the duration of each evaporation stage. However, when the biochar content increased to 2 % and 4 %, the completion time of the second evaporation stage was noticeably prolonged. Specifically, compared with the control group (43 h), the second-stage completion time of the 2 % and 4 % biochar treatments was prolonged by 9.3 % and 18.6 % respectively. Overall, biochar addition effectively inhibit water evaporation, particularly at higher application rates, by delaying the evaporation process and enhancing the water retention capacity of the samples.

As shown in Fig. 6a-c, when the content of biochar remained at 0 %, after the first dry-wet cycle, the residual moisture contents of the samples with 5 % and 10 % fly ash content were 5.706 ± 0.15 % and 6.464 ± 0.11 %, respectively. Compared with the control group (residual moisture content of 4.326 %), the samples with 5 % and 10 % fly ash content increased their residual moisture content by 31.90 % and 49.42 % respectively after the first cycle. With the increase of the number of dry-wet cycles, the residual moisture content of all samples showed a downward trend. After the fifth dry-wet cycle, the residual moisture contents of the samples with 5 % and 10 % fly ash content in the fifth cycle were 4.652 ± 0.248 % and 5.658 ± 0.201 %, respectively. Compared with their residual moisture contents after the first cycle, they decreased by 18.47 % and 12.47 % respectively, with the reduction being <23.15 % of the control group. The addition of fly ash can

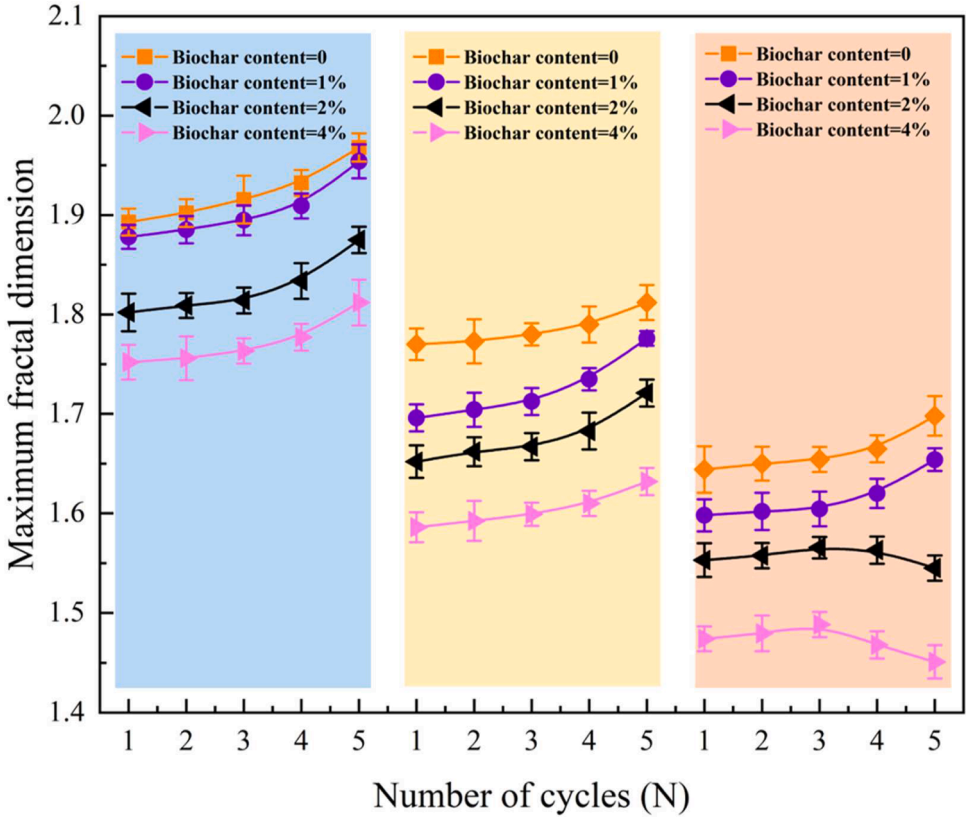

Fig. 8. Maximum fractal dimension of different treatments across wet–dry cycles. Error bars represent SEM ($n = 2$) (a) Fly ash content maintained at 0 %; (b) fly ash content maintained at 5 %; (c) fly ash content maintained at 10 %.

enhance the water retention capacity of the samples and slow down the water loss during the dry-wet cycle process.

As shown in Fig. 7d, when the content of biochar remained at 0 %, the addition of fly ash significantly affected the evaporation process of the samples. The duration of the first evaporation stage of the control group was 29 h, and the second stage was 14 h. Compared with this, the samples with 5 % and 10 % fly ash content had their first evaporation stage duration extended to 43 h and 95 h respectively, and the average evaporation rate in the first stage was reduced by 32.39 % and 64.54 % respectively. Correspondingly, the duration of the second stage also extended to 18 h and 22 h respectively. The addition of fly ash can effectively delay the evaporation process, reduce the initial evaporation rate, and prolong the duration of each evaporation stage, thereby significantly enhancing the water retention capacity of the samples in a dry environment.

As shown in Fig. 6b,c, when both biochar and fly ash were added, under the same biochar content and the same number of dry-wet cycles, the residual moisture content of the samples increased with the increase of fly ash content. As shown in Fig. 6c, taking the first dry-wet cycle as an example, when the fly ash content remained at 10 %, the samples with biochar contents of 1 %, 2 %, and 4 % had residual moisture contents of 7.546 ± 0.156 %, 7.884 ± 0.132 %, and 8.896 ± 0.174 % respectively. Compared with the sample with 10 % fly ash added alone (residual moisture content of 6.464 ± 0.112 %), the residual moisture content increased by 16.74 %, 21.97 %, and 37.62 % respectively after the combined addition of biochar. After the fifth dry-wet cycle, the residual moisture content of the sample with 10 % fly ash alone was 5.658 ± 0.202 %, while the residual moisture contents of the samples with 1 %, 2 %, and 4 % biochar added in combination were 7.68 ± 0.124 %, 8.15 ± 0.128 %, and 8.012 ± 0.162 % respectively, which were 35.74 %, 44.04 %, and 41.60 % higher than that of the sample with 10 % fly ash alone.

When the biochar content was fixed at 4 % (residual moisture content after the first cycle: 6.192 ± 0.167 %), the combined addition of 5 % and 10 % fly ash increased the residual moisture content to 7.262 ± 0.167 % and 8.896 ± 0.174 % respectively, representing increases of 17.28 % and 43.67 % relative to the single-biochar treatment. After the fifth cycle, the residual moisture content of the single 4 % biochar treatment was 5.123 ± 0.173 %, whereas the addition of 5 % and 10 % fly ash increased this value to 6.255 ± 0.139 % and 8.012 ± 0.162 %, respectively, corresponding to increases of 22.10 % and 56.39 % compared with the single-biochar treatment.

Notably, the composite treatment containing 4 % biochar content and 10 % fly ash consistently exhibited the highest residual moisture content under identical dry–wet conditions, indicating a strong synergistic water-retention effect between the two amendments. Taking the first cycle as an example, the residual moisture content of this composite sample (8.896 ± 0.174 %) was 105.64 % higher than that of the control group (4.326 ± 0.168 %). For example, based on the individual effects of 4 % biochar alone (+43.11 %) and 10 % fly ash alone (+49.42 %), the expected additive increase relative to the control would be approximately 92.53 %, whereas the observed increase for the combined treatment is 105.64 %, indicating a pronounced synergistic enhancement far beyond the individual contributions of biochar or fly ash alone. The water retention capacity further increased with increasing mixing ratios of the two amendments.

As shown in Fig. 7a–c, at the end of the second evaporation stage, the completion time of the control group was 43 h, whereas samples with single addition of 4 % biochar or 10 % fly ash, as well as the composite addition of 4 % biochar and 10 % fly ash, exhibited extended completion times of 51 h, 117 h, and 123 h, respectively. Compared with the 10 % fly ash treatment, which showed the best performance among single-material amendments (117 h), the evaporation process of the composite treatment was further prolonged by approximately 5.13 %. This result indicates that, under the synergistic action of biochar and fly ash,

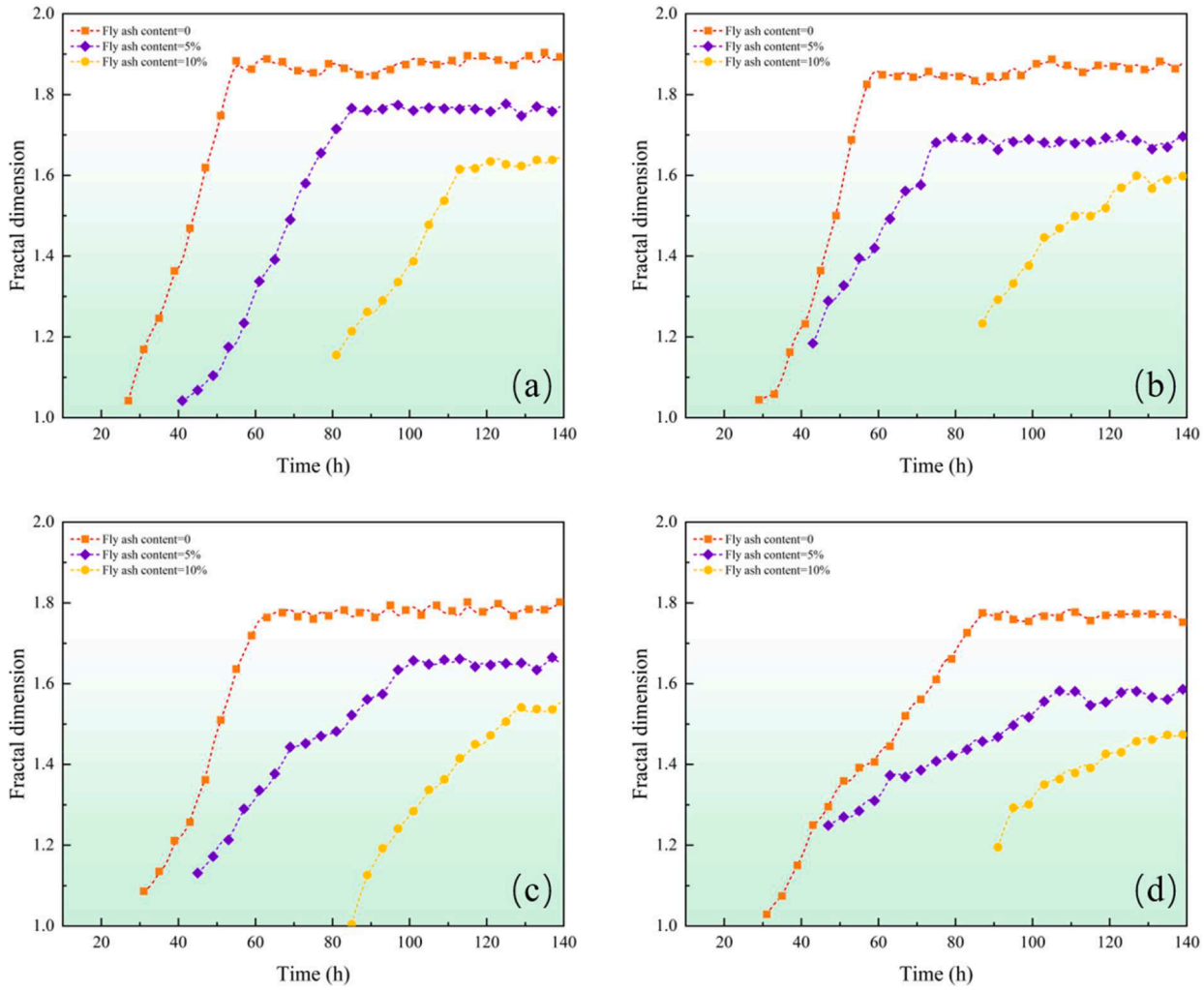

Fig. 9. Temporal evolution of the fractal dimension of the improved soil. (a) Fly ash content maintained at 0 %; (b) fly ash content maintained at 5 %; (c) fly ash content maintained at 10 %; (d) biochar content maintained at 0 %.

water evaporation can be more effectively delayed, and the water retention capacity of the treatment can be significantly enhanced compared with that of single-material amendments.

3.2. Fractal characteristics of cracks in molybdenum tailings soil remediated with fly ash biochar under dry-wet cycling conditions

As shown in Fig. 8a, when the fly ash content remained at 0 %, the maximum fractal dimension of the samples gradually decreased with increasing biochar content throughout the entire wet–dry cycling process. After the first cycle, the sample containing 4 % biochar exhibited the lowest fractal dimension (1.752 ± 0.018), which was 7.45 % lower than that of the control group (1.893 ± 0.014). By the end of the fifth dry–wet cycle, the corresponding fractal dimension (1.891 ± 0.015) was 7.93 % lower than that of the control group (2.064 ± 0.016). During the dry–wet cycling process, the fractal dimension of the control group increased by 3.9 % from the first to the fifth cycle, whereas the corresponding increase for the 4 % biochar treatment was 3.4 %, which was slightly lower than that of the control group. These results indicate that, in the absence of fly ash, biochar addition can partially delay the increase in fracture complexity induced by dry–wet cycling and reduce the rate of fractal dimension growth.

As shown in Fig. 8, when the biochar content remained at 0 %, the maximum fractal dimension of the sample decreased significantly with the increase in the fly ash content. After the first dry-wet cycle, the samples containing 5 % and 10 % fly ash content had fractal dimensions that were 6.5 % and 13.15 % lower than that of the control group, respectively. By the end of the fifth dry-wet cycle, the reduction was 7.9 % and 13.72 %, respectively. During the dry-wet cycling process, the fractal dimensions of the samples with 5 % and 10 % fly ash content increased by 2.37 % and 3.28 % respectively compared to their respective first cycle values, with the increase being less than that of the control group (3.9 %). This indicates that fly ash can also effectively inhibit the development of fracture networks.

Compared with the addition of biochar or fly ash alone, the combined improvement effect of biochar and fly ash is more significant. Among all treatments, the combination of 4 % biochar and 10 % fly ash exhibited the best performance. Taking the first dry–wet cycle as an example, the fractal dimension of the sample with this combination was 1.474 ± 0.124, which was 28.43 % lower than that of the control group (1.893 ± 0.014), representing a reduction substantially greater than that achieved with 4 % biochar alone (7.45 %) or 10 % fly ash alone (13.72 %). After five dry–wet cycles, the fractal dimension of this combined treatment was 1.56 % lower than that observed after the first cycle, indicating negative growth, whereas the control group increased by 3.9 %, and the treatment with 4 % biochar and 10 % fly ash alone also increased by 3.4 % and 3.28 % respectively. The combined improvement effect was significantly superior to that of single amendments, as it effectively inhibited the initiation, expansion, and increasingly complexity of fractures during the dry–wet cycling, thereby delaying soil

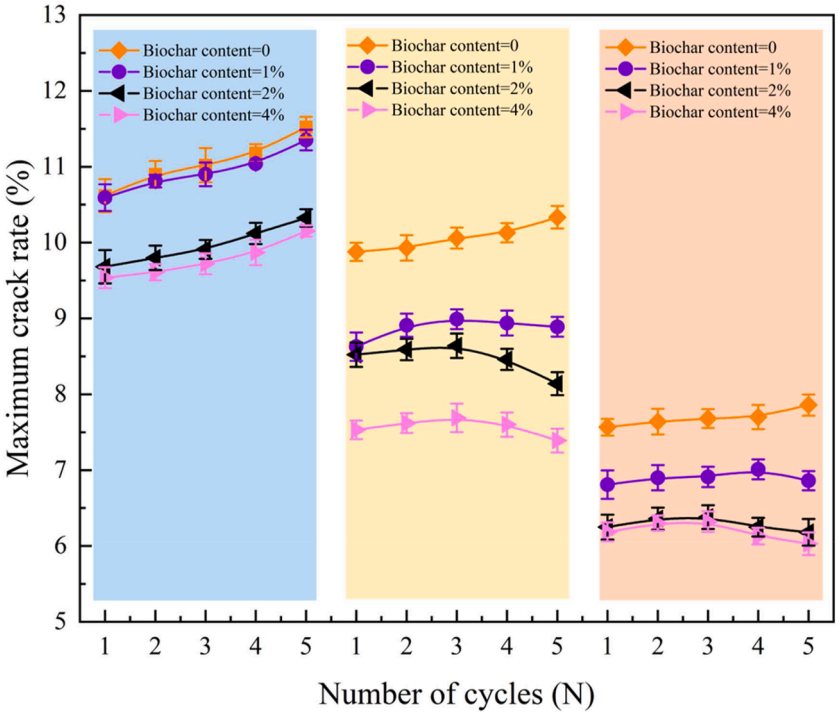

Fig. 10. Maximum crack rate of different treatments across wet–dry cycles. Error bars represent SEM ($n = 2$) (a) Maintain a fly ash content of 0 %; (b) Maintain a fly ash content of 5 %; (c) Maintain a fly ash content of 10 %.

structural degradation. Overall, the combination of 4 % biochar and 10 % fly ash represents the optimal treatment, as it not only significantly reduced the fractal dimension at the initial stage but also achieved negative growth in fracture development during dry–wet cycling, demonstrating excellent long-term structural stability.

As shown in Fig. 9, the temporal evolution curve of the fractal dimension can be divided into two typical stages: the first stage corresponds to crack initiation and rapid development, during which the fractal dimension increases sharply; the second stage represents a relatively stable crack period, during which the fractal dimension tends to stabilize and no longer increases significantly. The first stage is mainly driven by internal stress differences induced by initial dehydration, resulting in the rapid initiation and expansion of cracks; as time progresses, this stress gradually redistributes and approach equilibrium, and crack development enters the second stage, in which the expansion rate significantly decreases and eventually stabilizes.

Fig. 9 shows that both that single additions of biochar or fly ash and their combined application can delay the onset time of crack occurrence. When the biochar content remained at 0 %, the addition of fly ash significantly delayed crack initiation; compared with the sample without fly ash, the crack appearance time of samples containing 5 % and 10 % fly ash was delayed by 14 h and 40 h, respectively. Similarly, when the fly ash content remained at 0 %, increasing biochar content also slowed the initial crack development rate and delayed crack initiation; for example, the sample containing 4 % biochar exhibited a crack appearance time delayed by 4 h compared with the control group. For the composite treatment, the delaying effect was more pronounced: compared with the control group, the crack appearance was significantly extended to 91 h for the 4 % biochar + 10 % fly ash combination, indicating a clear synergistic effect between the two additives in inhibiting early crack formation.

The above results indicate that both biochar and fly ash can delay crack occurrence, with fly ash content exerting a more pronounced influence on crack appearance time: when biochar content remains constant, increasing fly ash content significantly delays crack initiation, whereas when fly ash is fixed, variations in biochar content have a comparatively smaller effect on crack appearance time. When the two amendments are applied in combination, changes in fly ash content remain the dominant factor controlling crack appearance time. Overall, the two stages of the fractal dimension curve correspond clearly to crack evolution behavior: the first stage (rapid rising segment) represents crack initiation and expansion, whereas the second stage (plateau segment) reflects stabilization of the crack network.

3.3. *Crack development characteristics of fly ash biochar-remediated molybdenum tailings soil under dry-wet cycling conditions*

As shown in Fig. 10a, when fly ash content remained at 0 %, the maximum crack rate of the samples gradually decreased with increasing biochar content. Among these treatments, the sample containing 4 % biochar exhibited the lowest crack rate, measuring 9.536 ± 0.138 % after the first wet–dry cycle and increasing to 10.152 ± 0.075 % by the end of the fifth cycle. Compared with the control group (first cycle: 10.618 ± 0.22 %, fifth cycle: 11.523 ± 0.136 %), the crack rate of this treatment decreased by 10.19 % and 11.90 % in the first and fifth wet–dry cycles, respectively.

Similarly, as shown in Fig. 10, when biochar content remained at 0 %, the maximum crack rate of the samples decreased significantly with the increase of the content of fly ash. Compared with the control group, the samples with 5 % and 10 % fly ash had crack rates that decreased by 7 % and 28.74 % respectively after the first dry-wet cycle; by the end of the fifth dry-wet cycle, the crack rate of the sample with 10 % fly ash decreased the most, reaching 31.81 %.

As shown in Figs. 10b, c, when biochar and fly ash were applied in combination, the inhibitory effect on crack development was further enhanced. Among all treatment combinations, the combination of 4 % biochar and 10 % fly ash exhibited the strongest inhibitory effect. The crack rate of this treatment after the first wet–dry cycle was 6.185 ± 0.125 %, which was 41.75 % lower than that of the control group; by the end of the fifth cycle, the crack rate decreased to 6.03 ± 0.149 %, representing a reduction of 47.67 % relative to the control group. Throughout the wet–dry cycling process, the crack rate of this composite

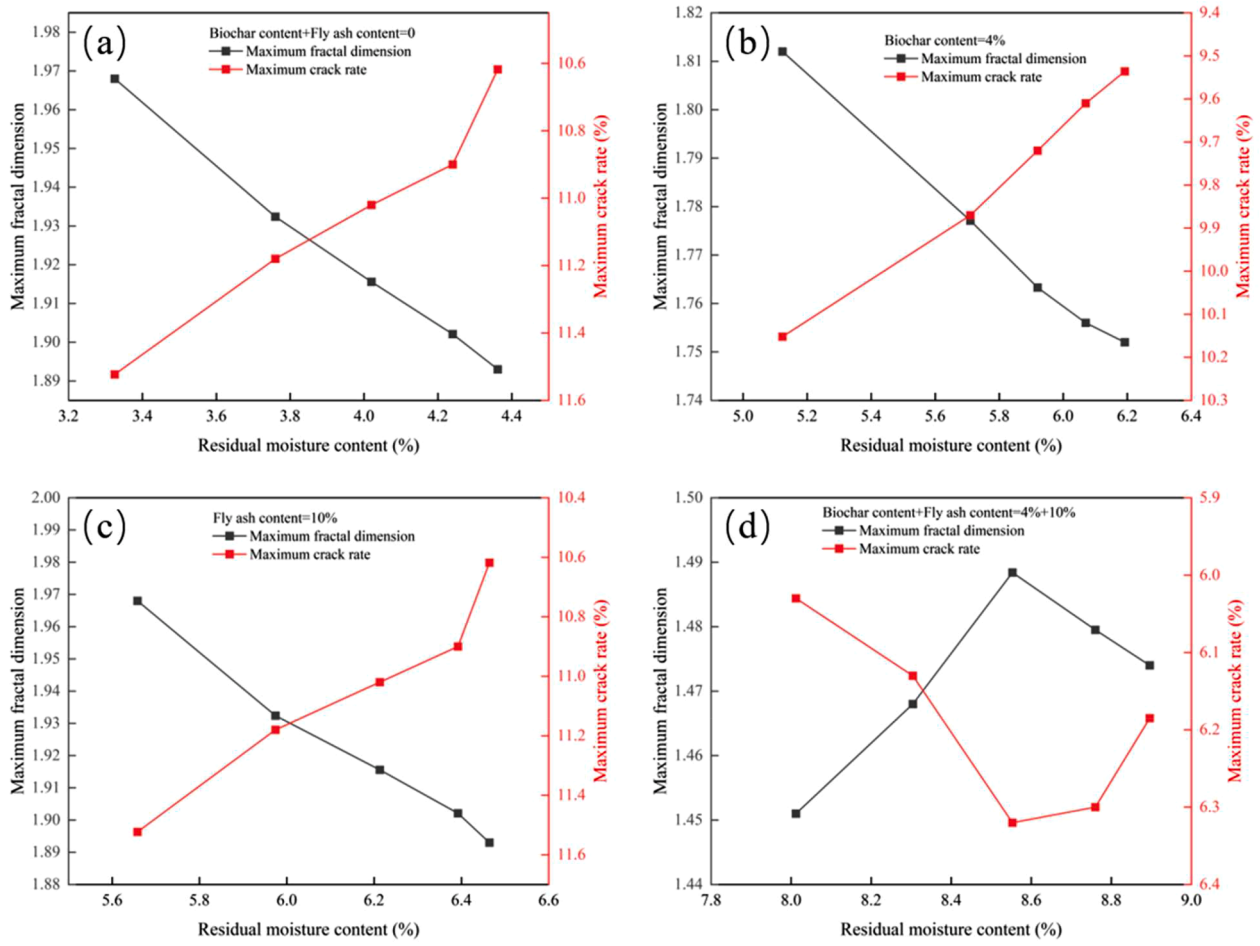

Fig. 11. Relationship between residual moisture content, maximum fractal dimension, and Crack rate of soil under different fly ash and biochar treatments after five wet dry cycles. (a) Without adding fly ash and biochar; (b) The biochar content is 4 %, and the fly ash content is 0 %; (c) The fly ash content is 10 %; Biochar content is 0 %; (d) Biochar and coal powder are added in a composite manner, with contents of 4 % and 10 %, respectively.

treatment consistently remain lower than those of the single-material treatments and the control group, demonstrating a clear advantage of synergistic improvement.

As shown in Fig. 11, the evolution of soil properties during the wet–dry cycling process exhibits significant differences among the various improvement strategies. For the control group without any amendments and the samples amended with a single additive (fly ash or biochar), a consistent negative correlation was observed after five wet–dry cycles: both the maximum fractal dimension and the maximum crack rate decreased with increasing residual water content.

In contrast, samples amended with both biochar and fly ash exhibited a more complex and nonlinear relationship with the wet–dry cycling process. During the first three cycles, the fractal dimension increased with increasing water content, whereas the crack rate exhibited the opposite trend. This pattern was reversed during the final two cycles. This transformation highlights how the composite amendment dynamically alters soil responses over time, effectively reorganizes soil structure to inhibit crack expansion, and significantly enhances water retention capacity.

In the fifth wet–dry cycle, the synergistic effect of the composite material (4 % biochar + 10 % fly ash) became quantitatively evident. Its performance was significantly superior to that all other groups across key indicators: it maintained the highest residual water content (8.012 %), achieved the lowest fractal dimension (1.451), and exhibited the lowest crack rate (6.03 %). Compared with the control group (3.325 %, 1.968 %, 11.523 %), the residual water content increased by approximately 140.9 %, whereas the fractal dimension and crack rate decreased by approximately 26.3 %, and 47.6 %, respectively. This composite treatment also outperformed the best single-additive treatment, confirming that the combined use of biochar and fly ash provides more comprehensive improvements in soil structural stability and hydrological functions than either material used alone.

As shown in Fig. 12a, when biochar content remained at 0 %, the fracture ratio of the samples decreased with the increase in the content of fly ash. Compared with the control group, the fracture ratios of the samples with 5 % and 10 % fly ash added decreased by 7.12 % and 28.74 %, respectively. Similarly, as shown in Fig. 12, when the content of fly ash remained at 0 %, increasing the content of biochar also led to a decrease in the crack density of the specimens. Increasing the content of biochar can also effectively reduce the fracture ratio. For example, the average fracture ratio of the sample with 4 % biochar added was 10.19 % lower than that of the control group. Among all the specimens, the control group with no modifier had the highest fracture ratio (10.6), while the composite specimen with 4 % biochar and 10 % fly ash added had the lowest fracture ratio (6.14).

In conclusion, both biochar and fly ash effectively inhibited crack development. Notably, when biochar content was fixed, the crack rate decreased significantly with increasing fly ash content; conversely, when fly ash content was fixed, variations in biochar content had a relatively limited effect on the crack rate.

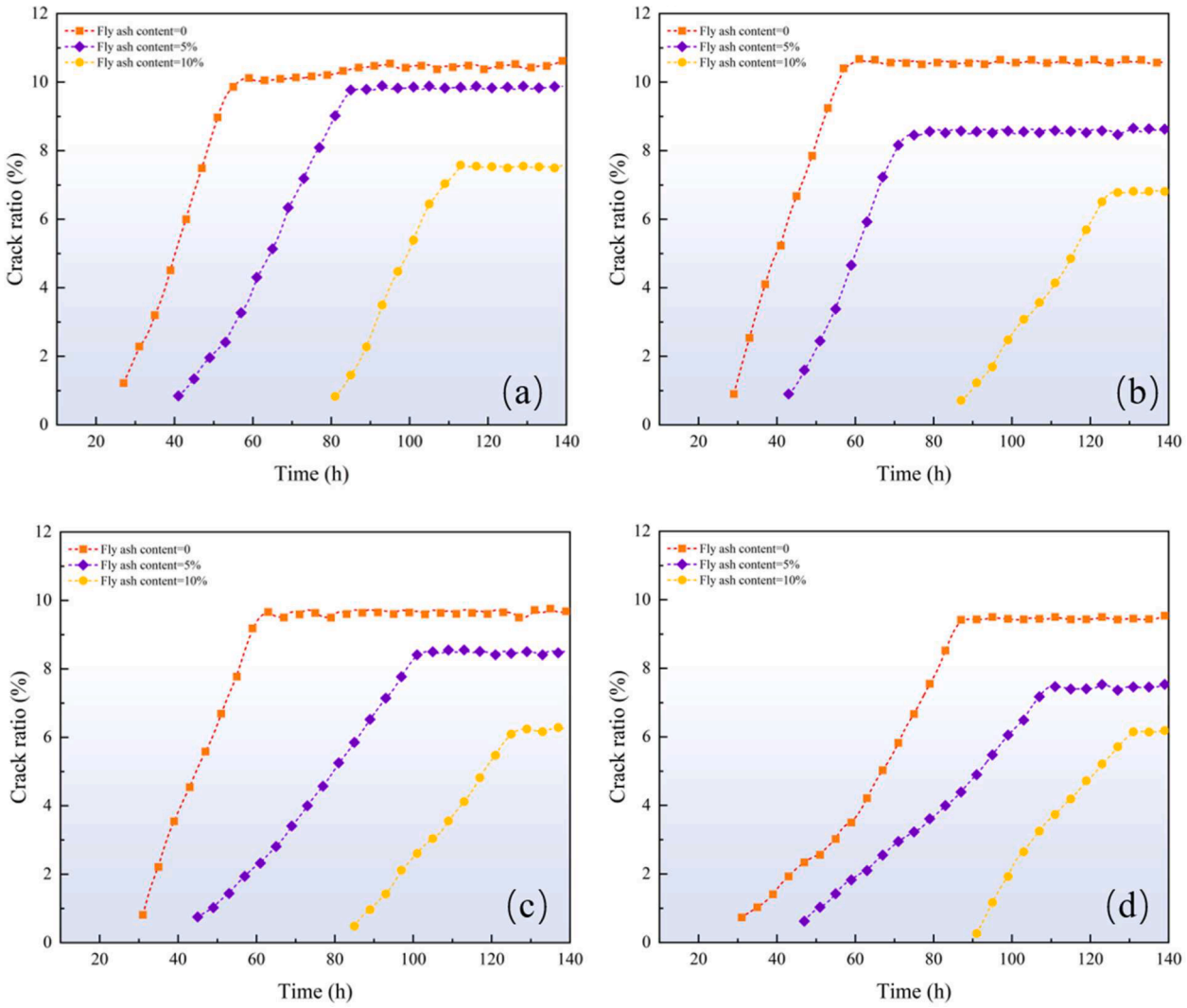

Fig. 12. The variation of crack rate over time during the process of improving soil drying. (a) Biochar content maintained at 0 %; (b) biochar content maintained at 1 %; (c) biochar content maintained at 2 %; (d) biochar content maintained at 4 %.

4. Discussion

4.1. Synergistic suppression of cracking in molybdenum tailings soil by fly ash and biochar during drought rainfall

As shown in Fig. 13, when biochar content remained at 0 %. The number of crack nodes in the samples gradually decreased with increasing fly ash content. Among all treatments, the sample containing 10 % fly ash exhibited the lowest final number of crack nodes, representing a reduction of 32.56 % relative to the control group. When fly ash content remained at 0 %, the number of crack nodes in the samples decreased with increasing biochar content. Compared with the control group, the final number of crack nodes in samples containing 1 %, 2 %, and 4 % biochar decreased by 13.95 %, 18.14 %, and 48.84 % respectively. When biochar and fly ash were applied in combination, the inhibitory effect on crack node formation was significantly enhanced. Among all combinations, the composite treatment comprising 4 % biochar and 10 % fly ash exhibited the most pronounced effect, with the final number of crack nodes reduced by 59.53 % relative to the control group.

As shown in Fig. 14, uneven internal stress distribution within the soil is one of the primary causes of crack initiation. When soil undergoes drying-induced contraction due to water loss or external loading, cracks are more likely to form. These initial primary cracks gradually thicken, extend, and widen over time, from which secondary and tertiary cracks develop, collectively forming a complex crack network that comprises soil structural integrity.

Fly ash and biochar are fine-grained materials that can effectively fill soil pores and reduce local stress concentrations, thereby minimizing the formation of primary crack nodes. Fly ash that has undergone alkalization treatment and can react with water to generate cementitious substances. These cementitious substances can bind soil particles and biochar together, thereby enhancing overall structural stability. Biochar has a highly porous structure and can reduce water loss during soil drying [48–49]. This process alleviates the shrinkage caused by stress redistribution and continuously provides a favorable internal environment for fly ash hydration reactions, thereby promoting the formation of cementitious substances. Consequently, the development of secondary and tertiary cracks is suppressed, resulting in a reduced number of crack nodes.

This synergistic interaction significantly enhances the fracture toughness and crack resistance of the soil matrix. During crack propagation, the reinforced cementation system formed by biochar, fly ash, and soil inhibits the uneven stress distribution. The combined cementation and pore-filling effects improve soil structural integrity, thereby requiring higher stress to levels to initiate new cracks. Consequently, the development of primary cracks is restricted, and the number, length, and connectivity of secondary and tertiary cracks are significantly

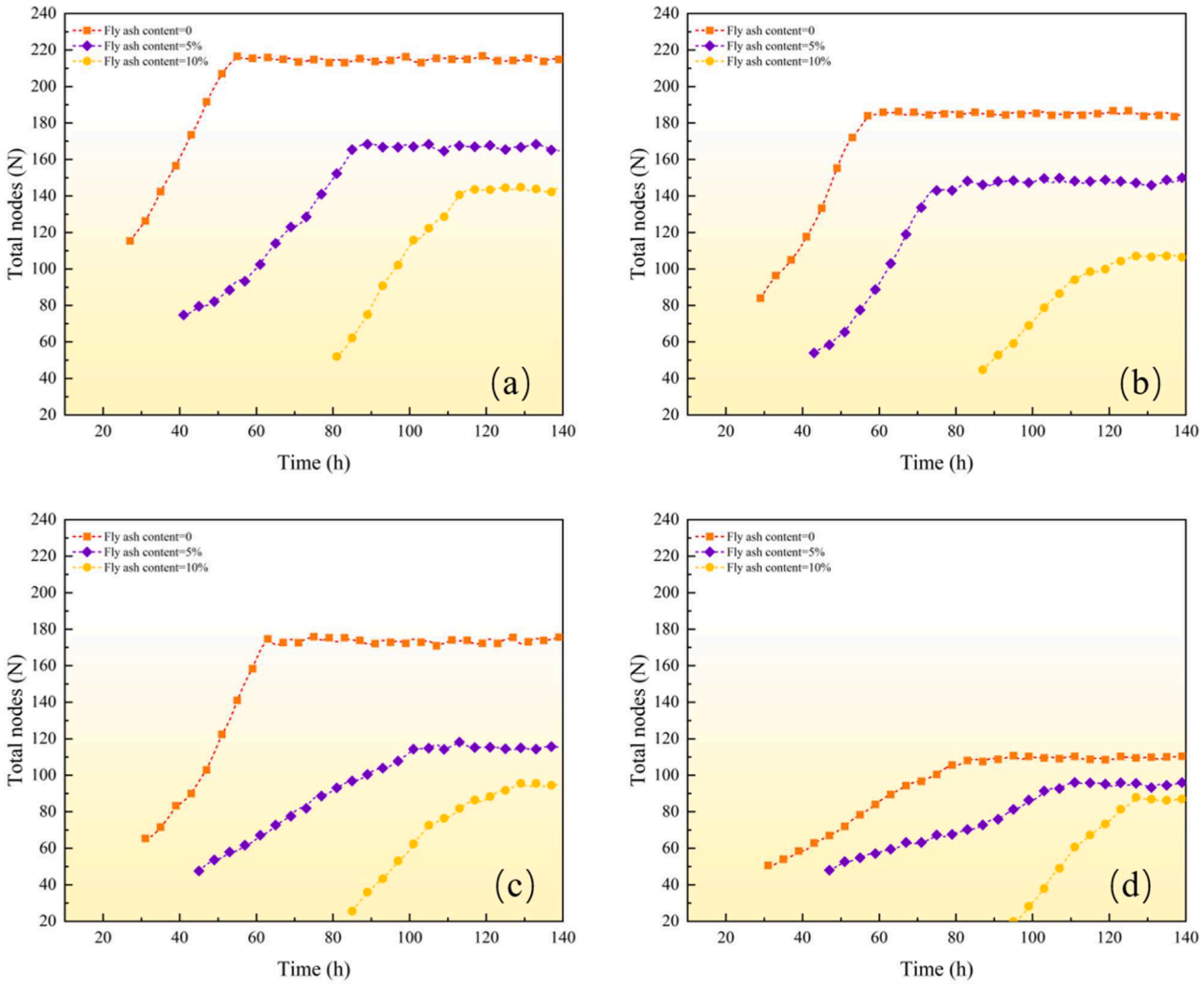

Fig. 13. Temporal variation in the number of crack nodes during drought in the remediation process of molybdenum tailings soil. (a) Biochar content maintained at 0 %; (b) biochar content maintained at 1 %; (c) biochar content maintained at 2 %; (d) biochar content maintained at 4 %.

reduced. Eventually, the overall fracture network tends to simplify and become more intact, manifesting macroscopically as a less fractured pattern with fewer crack nodes (Fig. 14). However, although fly ash can inhibit soil cracking, excessive addition may introduce the risk of heavy metal contamination [50]. Therefore, when fly ash is used to improve tailings soil, careful consideration of the balance between application rate and potential environmental impacts is required to avoid secondary environmental problems arising from improper treatment.

It should be emphasized that the mechanistic interpretation proposed here—involving pore filling and cementation—is inferred from SEM morphological observations and consistency with literature on fly ash and biochar amended soils, rather than from direct chemical or mineralogical identification. Future work combining micro-CT, XRD, and SEM–EDS is required to confirm the nature and continuity of the cementitious networks inferred from our data.

4.2. Synergistic enhancement of mo tailings soil water retention by fly ash and biochar during drought–rainfall events

As shown in Fig. 15, soil water evaporation mainly consists of three distinct stages. The addition of fly ash and biochar significantly affects evaporation across these stages through synergistic physical and chemical mechanisms, ultimately enhancing soil water retention capacity. During the stable rapid evaporation stage, water transport occurs mainly through the soil surface layer. The results indicate that the addition of biochar and fly ash significantly prolongs this stage. For example, compared with the control group, the addition of 10 % fly ash extended the duration of the first stage by 66 h (Fig. 7). Correspondingly, the average evaporation rate decreases by 64.54 %. This significant delay can be attributed to the physical filling of soil pores by fine fly ash and biochar particles, which hinders rapid water migration pathways. Chemically, fly ash hydration forms cementing substance that promote soil aggregation and reduce the exposed water surface area, thereby slowing the initial evaporation rate.

During the evaporation deceleration stage, the soil's internal water evaporation capacity gradually weakens. Biochar, owing to its well-developed porous structure, effectively inhibits water loss during the drying process. Data show that, for samples containing 4 % biochar, the end time of the evaporation deceleration stage was 51 h longer than that of the control group. Fly ash exerts a water-retaining effect primarily through chemical reactions. For samples containing 10 % fly ash, this stage was prolonged by 117 h. This mechanism lies in the formation of cementing substances through fly ash reactions, which tightly bind soil particles, enhance aggregate stability, and make water outflow more difficult. With the filling of the soil structure by the combined effects of biochar and fly ash, the soil matrix becomes more compact. This significantly inhibits crack development induced by drying shrinkage and prevents secondary evaporation associated with crack formation.

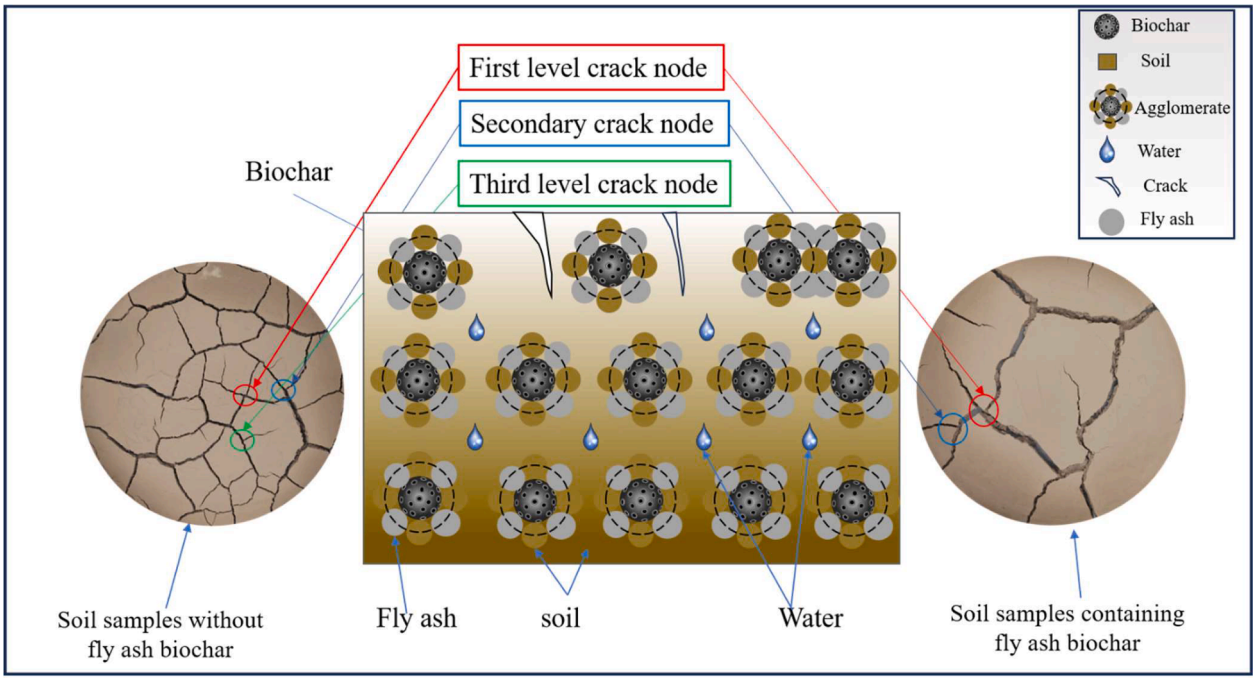

Fig. 14. Schematic diagram of the synergistic crack suppression mechanism of Biochar and Fly ash.

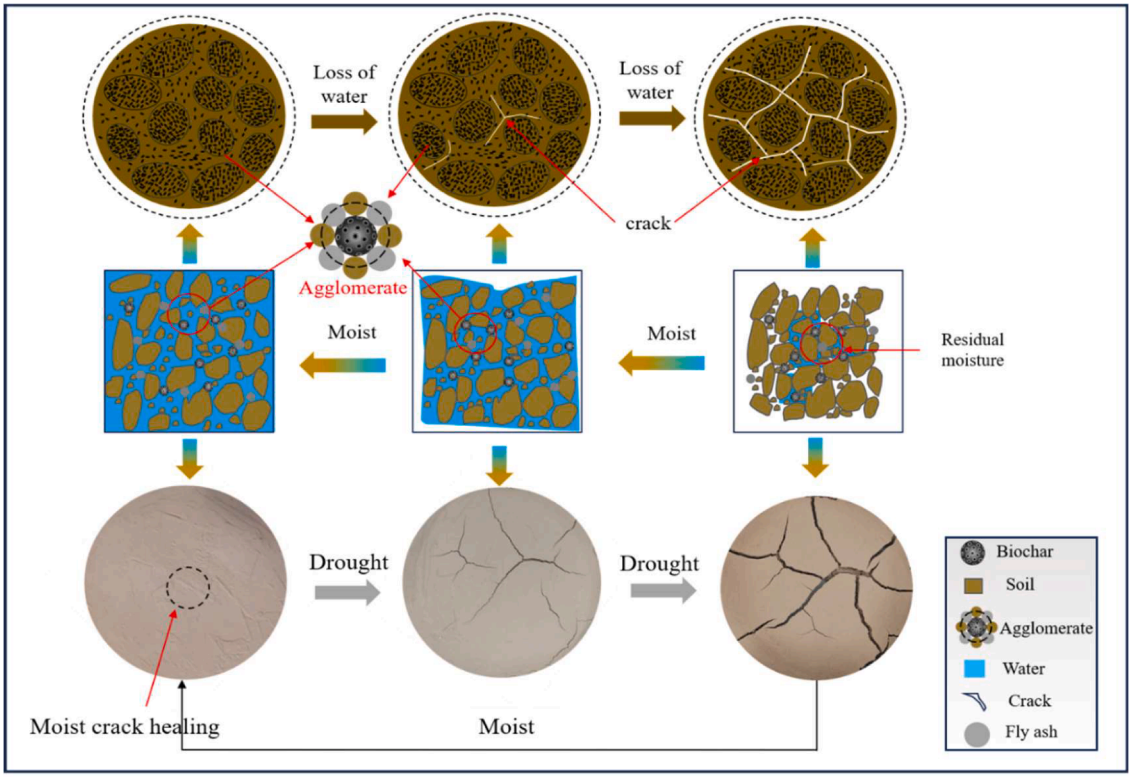

Fig. 15. Water retention characteristics of amended soil under wet–dry cycling.

Consequently, this leads to a smoother and more gradually decelerating evaporation process.

After entering the residual evaporation stage, the final residual water content of the amended samples was significantly higher, representing a key quantitative finding illustrated in Fig. 6. For example, after the first wet–dry cycle, the combination of 10 % fly ash and 4 % biochar resulted in final residual water content that was 103.94 % higher than that of the control group. This excellent water retention performance under low-moisture conditions can be explained by the combined effects of fly ash filling pores and reducing crack connectivity, together with biochar's ability to retain bound water within its porous structure. Consequently, evaporation during this stage occurred at an extremely low rate over an extended period, as demonstrated by the prolonged time required to reach water balance—from 43 h in the control group to 123

h for samples containing 4 % biochar and 10 % fly ash (Fig. 7). This prolonged drying process highlights the effectiveness of the amendments in enhancing soil long-term water retention. From an engineering perspective, the 10 % fly ash + 4 % biochar treatment corresponds to approximately 80 kg/m^3 of tailings, which is feasible for surface layers, reclamation covers, but cost and long-term heavy-metal leaching behavior must be evaluated at pilot scale.

5. Conclusion

This study confirms that the combined addition of biochar and fly ash exerts a significant synergistic improvement effect on the water retention and crack resistance of molybdenum tailings soil under wet–dry cycling conditions. Among the tested treatments, the combination of 4 % biochar and 10 % fly ash represents the optimal ratio, significantly increasing the final residual water content of the soil by 105.64 % after the first wet–dry cycle. Under this treatment, the fractal dimension and crack rate were significantly reduced by 28.43 % and 41.75 % respectively. After five wet–dry cycles, its crack resistance advantage further increased, with the crack rate decreasing by 47.67 %, and the fractal dimension exhibiting negative growth (−1.56 %). In contrast, both the control group and the single-material treatment groups exhibited positive growth in fractal dimension.

This synergistic effect arises from dual mechanisms of physical filling and chemical bonding: fine-grained materials fill pores and slow water evaporation, while cementitious substances formed during fly ash hydration tightly bind soil particles and porous biochar, substantially enhancing aggregate stability and structural integrity, thereby effectively inhibiting crack initiation and network complexity and reducing the number of crack nodes by 59.53 %. This amendment ratio provides a feasible remediation strategy for improving the structural stability of molybdenum tailings soil in arid areas.

Future research needs to increase the number of experimental repetitions, and use advanced imaging techniques such as micro-CT to directly verify the spatial distribution of the bonding network, and evaluate its long-term ecological benefits and heavy metal fixation effects at the field scale and over a longer period.

CRediT authorship contribution statement

Binbin Yang: Writing – review & editing, Writing – original draft, Supervision, Investigation. **Mingming Hu:** Software, Investigation, Funding acquisition, Formal analysis, Data curation.

Declaration of competing interest

No conflict of interest exits in the submission of this manuscript, and manuscript is approved by all authors for publication. I would like to declare on behalf of my co-authors that the work described was original research that this paper is new, neither the entire paper nor any part of its content has been published or has been accepted elsewhere. It is not being submitted to any other journal.

Acknowledgments

This research was funded by Key Scientific Research Project of Colleges and Universities in Henan(25B410001), the National Natural Science Foundation of China (52364021) and Outstanding Youth Science Fund of Xinjiang Autonomous Region under (2025D01E20).

Data availability

Data will be made available on request.

References

[1] B. Talukder, N. Ganguli, R. Matthew, G.W. VanLoon, K.W. Hipel, J. Orbinski, Climate change-triggered land degradation and planetary health: a review, Land Degrad. Dev. 32 (16) (2021) 4509–4522, https://doi.org/10.1002/ldr.4056.
[2] K. Hermans, R. McLeman, Climate change, drought, land degradation and migration: exploring the linkages, Curr. Opin. Environ. Sustain. (2021) 236–244, https://doi.org/10.1016/j.cosust.2021.04.013.
[3] J. Wang, J. Zhen, W. Hu, S. Chen, I. Lizaga, M. Zeraatpisheh, X. Yang, Remote sensing of soil degradation: progress and perspective, Int. Soil Water Conserv. Res. (2023) 429–454, https://doi.org/10.1016/j.iswcr.2023.03.002.
[4] F.U. Iwuchukwu, U. Ewuzie, O.J. Ajala, V.E. Ojukwu, I.C. Nnorom, J.C. Egbueri, J. O. Ighalo, A consideration of the climatic drivers, focal points and challenges of soil erosion, land degradation, landslides and landscapes in Nigeria, Climate Change Impacts Nigeria: Environ. Sustain. Develop. (2023) 449–477, https://doi.org/10.1007/978-3-031-21007-523.
[5] N. Li, Y. Guo, L. Wang, Q. Wang, D. Yan, S. Zhao, T. Lei, Evaluation and quantitative characterization for the ecological environment impact of open pit mining on vegetation destruction from Landsat time series: a case study of Wulishan limestone mine, Ecol. Indic. (2024) 111371, https://doi.org/10.1016/j.ecolind.2023.111371.
[6] C. Zhang, L. Guo, J. Li, Q. Li, H. Kang, Y. Xu, S. Raval, Identifying the vegetation destruction and restoration in surface coal mines across China over the past three decades by EAuto-VDR, J. Environ. Manage. (2025) 126195, https://doi.org/10.1016/j.jenvman.2025.126195.
[7] Z. Long, Y. Huang, W. Zhang, Z. Shi, D. Yu, Y. Chen, C. Liu, R. Wang, Effect of different industrial activities on soil heavy metal pollution, ecological risk, and health risk, Environ. Monit. Assess. 20 (2021), https://doi.org/10.1007/s10661-020-08807-z.
[8] J.Y. Peng, S. Zhang, Y. Han, B. Bate, H. Ke, Y. Chen, Soil heavy metal pollution of industrial legacies in China and health risk assessment, Sci. Total Environ. (2022) 151632, https://doi.org/10.1016/j.scitotenv.2021.151632.
[9] P.B. Angon, M.S. Islam, A. Das, N. Anjum, A. Poudel, S.A. Suchi, Sources, effects and present perspectives of heavy metals contamination: soil, plants and human food chain, Heliyon (2024) e28712, https://doi.org/10.1016/j.heliyon.2024.e28357.
[10] L. Zhang, Y. Zhu, Y. Zhang, J. Zhong, J. Li, S. Yang, Y. Zhang, Characteristics, source analysis, and health risk assessment of potentially toxic elements pollution in soil of dense molybdenum tailing ponds area in central China, Environ. Geochem. Health (2024) 129, https://doi.org/10.1007/s10653-024-01886-8.
[11] W. Hui, Z. Hao, T. Hongyan, W. Jiawei, L. Anna, Heavy metal pollution characteristics and health risk evaluation of soil around a tungsten-molybdenum mine in Luoyang, China, Environ. Earth Sci. (2021) 293, https://doi.org/10.1007/s12665-021-09539-0.
[12] Z.Y. Chen, Y.Y. Zhao, D.L. Chen, H.T. Huang, Y. Zhao, Y.J. Wu, Ecological risk assessment and early warning of heavy metal cumulation in the soils near the Luanchuan molybdenum polymetallic mine concentration area, Henan Province, central China, China Geol. (2023) 15–26, https://doi.org/10.31035/cg2023003.
[13] N. Blenis, N. Hue, T.M. Maaz, M. Kantar, Biochar production, modification, and its uses in soil remediation: a review, Sustainability (2023) 3442, https://doi.org/10.3390/su15043442.
[14] A.I. Osman, S. Fawzy, M. Farghali, M. El-Azazy, A.M. Elgarahy, R.A. Fahim, M.I.A. A. Maksoud, A.A. Ajlan, M. Yousry, Y. Saleem, D.W. Rooney, Biochar for agronomy, animal farming, anaerobic digestion, composting, water treatment, soil remediation, construction, energy storage, and carbon sequestration: a review, Environ. Chem. Lett. (2022) 2385–2485, https://doi.org/10.1007/s10311-022-01424-x.
[15] S. Sánchez, D. Baragaño, J.R. Gallego, M.A. López-Antón, R. Forján, A. González, Valorization of steelmaking slag and coal fly ash as amendments in combination with Betula pubescens for the remediation of a highly as-and Hg-polluted mining soil, Sci. Total Environ. (2024) 172297, https://doi.org/10.1016/j.scitotenv.2024.172297.
[16] T. Tian, L. Yu, R. Feng, C. Yao, L. Gong, H. Xiao, L. Liu, F. Li, Unveiling the combined effects of water management and lime on remediation of Cd-contaminated soils with improved soil quality, J. Environ. Chem. Eng. (2024) 114778, https://doi.org/10.1016/j.jece.2024.114778.
[17] Z. Huang, H.Y. Sun, Y.M. Dai, P.B. Hou, W.Z. Zhou, L.L. Bian, A study on the shear strength and dry-wet cracking behaviour of waste fibre-reinforced expansive soil, case stud, Constr. Mater. (2022) e01142, https://doi.org/10.1016/j.cscm.2022.e01142.
[18] P.P. Das, K.R. Singh, G. Nagpure, A. Mansoori, R.P. Singh, I.A. Ghazi, A. Kumar, J. Singh, Plant-soil-microbes: a tripartite interaction for nutrient acquisition and better plant growth for sustainable agricultural practices, Environ. Res. (2022) 113821, https://doi.org/10.1016/j.envres.2022.113821.
[19] N.D. Nnaji, H. Onyeaka, T. Miri, C. Ugwa, Bioaccumulation for heavy metal removal: a review, SN Appl. Sci. 125 (2023), https://doi.org/10.1007/s42452-023-05351-6.
[20] T. Sladkovska, K. Wolski, H. Bujak, A. Radkowski, Ł. Sobol, A review of research on the use of selected grass species in removal of heavy metals, Agronomy (2022) 2587, https://doi.org/10.3390/agronomy12102587.
[21] P. Song, D. Xu, J. Yue, Y. Ma, S. Dong, J. Feng, Recent advances in soil remediation technology for heavy metal contaminated sites: a critical review, Sci. Total Environ. (2022) 156417, https://doi.org/10.1016/j.scitotenv.2022.156417.
[22] W. Zheng, T. Cui, H. Li, Combined technologies for the remediation of soils contaminated by organic pollutants. a review, Environ. Chem. Lett. (2022) 2043–2062, https://doi.org/10.1007/s10311-022-01407-y.

[23] K.A. Ghazaryan, H.S. Movsesyan, H.E. Khachatryan, N.P. Ghazaryan, Geochemistry of potentially toxic trace elements in soils of mining area: a case study from zangezur copper and molybdenum combine, armenia, Bull. Environ. Contam. Toxicol. (2018) 732–737, https://doi.org/10.1007/s00128-018-2443-0.
[24] J.C. Ribeiro Filho, E.M.D. Andrade, M.S. Guerreiro, H.A.D.Q. Palácio, J.B. Brasil, Soil–water–atmosphere effects on Soil crack characteristics under field conditions in a semiarid climate, Hydrology 83 (2023), https://doi.org/10.3390/hydrology10040083.
[25] H.Y. Fang, Soil-pollutant interaction effects on the soil behavior and the stability of foundation structures. Environmental geotechnics, CRC Press, Boca Raton, 2021, pp. 155–163.
[26] J. Xu, Y. Li, B. Wang, Z. Wang, S. Wang, Microstructure and permeability of bentonite-modified loess after wetting–drying cycles, Int. J. Geomech. (2023) 04023052, https://doi.org/10.1061/IJGNAI.GMENG-7726.
[27] T. Wen, K.H. Cheong, The fractal dimension of complex networks: a review, Inf. Fusion (2021) 87–102, https://doi.org/10.1016/j.inffus.2021.02.001.
[28] Y. Ding, Y. Liu, S. Liu, Z. Li, X. Tan, X. Huang, B. Zheng, Biochar to improve soil fertility. a review, Agron. Sustain. Dev. 36 (2016), https://doi.org/10.1007/s13593-016-0372-z.
[29] A. Kumar, T. Bhattacharya, S. Mukherjee, B. Sarkar, A perspective on biochar for repairing damages in the soil–plant system caused by climate change-driven extreme weather events, Biochar 22 (2022), https://doi.org/10.1007/s42773-022-00148-z.
[30] L. Luo, J. Wang, J. Lv, Z. Liu, T. Sun, Y. Yang, Y.G. Zhu, Carbon sequestration strategies in soil using biochar: advances, challenges, and opportunities, Environ. Sci. Technol. (2023) 11357–11372, https://doi.org/10.1021/acs.est.3c02620.
[31] I. Nogués, V.M. Miritana, L. Passatore, M. Zacchini, E. Peruzzi, S. Carloni, S. Marinari, Biochar soil amendment as carbon farming practice in a Mediterranean environment, Geoderma Reg. (2023) e00634, https://doi.org/10.1016/j.geodrs.2023.e00634.
[32] F. Linam, M.A. Limmer, A.M. Ebling, A.L. Seyfferth, Rice husk and husk biochar soil amendments store soil carbon while water management controls dissolved organic matter chemistry in well-weathered soil, J. Environ. Manage. (2023) 117936, https://doi.org/10.1016/j.jenvman.2023.117936.
[33] T.B. Nguyen, K. Sherpa, X.T. Bui, V.T. Nguyen, T.D.H. Vo, H.T.T. Ho, C.D. Dong, Biochar for soil remediation: a comprehensive review of current research on pollutant removal, Environ. Pollut. (2023) 122571, https://doi.org/10.1016/j.envpol.2023.122571.
[34] M. Qiu, L. Liu, Q. Ling, Y. Cai, S. Yu, S. Wang, X. Wang, Biochar for the removal of contaminants from soil and water: a review, Biochar 19 (2022), https://doi.org/10.1007/s42773-022-00146-1.
[35] L. Chen, F. Li, Y. Zhang, et al., Metal-organic-framework and walnut shell biochar composites for lead and hexavalent chromium removal from aqueous environments, Chemosphere (2024) 143572, https://doi.org/10.1016/j.chemosphere.2024.143572.
[36] K. Taweengern, S. Aramrak, C. Areeprasert, Field evaluation of biochar and fly ash as soil amendments for sugarcane cultivation on low-quality soils, Sci. Total Environ. (2025) 173000, https://doi.org/10.1016/j.biombioe.2025.108779.
[37] Y. Lu, K. Gu, Z. Shen, X. Wang, Y. Zhang, C.S. Tang, B. Shi, Effects of biochar particle size and dosage on the desiccation cracking behavior of a silty clay, Sci. Total Environ. (2022) 155788, https://doi.org/10.1016/j.scitotenv.2022.155788.
[38] D. Si, Y. Lin, Q. Xu, S. Zhang, Effects of biochar on rainwater redistribution, soil water evaporation and desiccation cracking: a case study of limestone soil in karst areas of southwest China, Sci. Total Environ. (2025) 178692, https://doi.org/10.1016/j.scitotenv.2025.178692.
[39] M.F. Noaman, M.A. Khan, K. Ali, A. Hassan, A review on the effect of fly ash on the geotechnical properties and stability of soil, Cleaner Mater. (2022) 100151, https://doi.org/10.1016/j.clema.2022.100151.
[40] A. Varshney, P. Dahiya, A. Sharma, R. Pandey, S. Mohan, Fly ash application in soil for sustainable agriculture: an Indian overview, Energy Ecol. Environ. (2022) 340–357, https://doi.org/10.1007/s40974-022-00241-w.
[41] Y. Zhang, E.J. Reardon, Removal of B, Cr, Mo, and Se from wastewater by incorporation into hydrocalumite and ettringite, Environ. Sci. Technol. (2003) 2947–2952, https://doi.org/10.1021/es020969i.
[42] M. Usman, I. Anastopoulos, Y. Hamid, A. Wakeel, Recent trends in the use of fly ash for the adsorption of pollutants in contaminated wastewater and soils: effects on soil quality and plant growth, Environ. Sci. Pollut. Res. (2023) 124427–124446, https://doi.org/10.1007/s11356-022-19192-0.
[43] Y. Ma, X. Shang, Y. Zhang, W. Chen, Y. Gao, J. Guo, H. Zheng, B. Xing, Co-pyrolysis of alkali-fused fly ash and corn stover to synthesize biochar composites for remediating lead-contaminated soil, Environ. Res. (2024) 118938, https://doi.org/10.1016/j.envres.2024.118938.
[44] D. Xu, P. Ji, L. Wang, X. Zhao, X. Hu, X. Huang, H. Zhao, F. Liu, Effect of modified fly ash on environmental safety of two soils contaminated with cadmium and lead, Ecotoxicol. Environ. Saf. (2021) 112175, https://doi.org/10.1016/j.ecoenv.2021.112175.
[45] F. Yan, H. Zhao, F. Liu, L. Wang, X. Huang, X. Zhao, Y. Yang, J. Li, G. Zhang, X. Ju, F. Wu, P. Ji, Remediation of cadmium and lead in contaminated soils by a newly modified fly ash material: the possibility and safety, Environ. Technol. Innov. (2022) 102894, https://doi.org/10.1016/j.eti.2022.102894.
[46] B. Yang, J. Liu, X. Zhao, S. Zheng, Evaporation and cracked soda soil improved by fly ash from recycled materials, Land Degrad. Dev. (2021) 2823–2832, https://doi.org/10.1002/ldr.3966.
[47] R. Gahlot, A. Verma, M. Kumar, Geotechnical behavior of fly ash-coal ash and bentonite clay composite as a landfill barrier material with special emphasis on desiccation cracks, Environ. Res. (2022) 113853, https://doi.org/10.1016/j.envres.2022.113853.
[48] F. Srocke, L. Han, P. Dutilleul, X. Xiao, D.L. Smith, O. Mašek, Synchrotron X-ray microtomography and multifractal analysis for the characterization of pore structure and distribution in softwood pellet biochar, Biochar (2021) 671–686, https://doi.org/10.1007/s42773-021-00104-3.
[49] C. Huang, Y. Chen, L. Jin, B. Yang, Properties of biochars derived from different straw at 500 °C pyrolytic temperature: implications for their use to improving acidic soil water retention, Agric. Water Manag. (2024) 108953, https://doi.org/10.1016/j.agwat.2024.108953.
[50] J. Horvatinec, J. Buczny, G. Ondrasek, Fly ash application impacts master physicochemical pedovariables: A multilevel meta-analysis, J. Environ. Manage. (Sep. 2024) 122066, https://doi.org/10.1016/j.jenvman.2024.122066.